

*Handwritten signature*

WVT-TR-76040

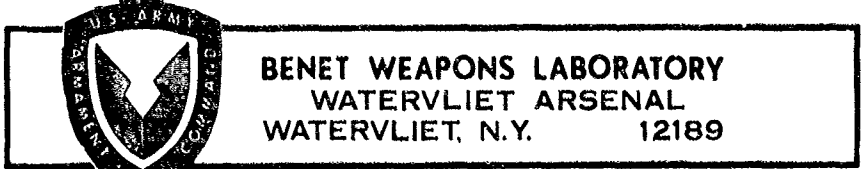
AD

ADA033370

STRESS INTENSITY FACTORS FOR A PRESSURIZED THICK-WALL  
CYLINDER WITH A PART-THROUGH CIRCULAR SURFACE FLAW -  
COMPLIANCE CALIBRATION AND COLLOCATION METHOD

M. A. Hussain  
J. F. Throop  
S. L. Pu  
R. D. Scanlon

October 1976



**BENET WEAPONS LABORATORY**  
**WATERVLIET ARSENAL**  
**WATERVLIET, N.Y. 12189**

**TECHNICAL REPORT**

AMCMS No. 511102.11.H5400

DA Project No. 1T161102AH54

*Handwritten notes and signatures*

DISPOSITION

Destroy this report when it is no longer needed. Do not return it to the originator.

DISCLAIMER

The findings in this report are not to be construed as an official Department of the Army position unless so designated by other authorized documents.

REPORT DOCUMENTATION PAGE		READ INSTRUCTIONS BEFORE COMPLETING FORM	
1. REPORT NUMBER WAT-TR-76048	2. GOVT ACCESSION NO.	3. REGISTRY'S CATALOG NUMBER ②	
4. TITLE (and Subtitle) Stress Intensity Factors for a Pressurized Thick-Walled Cylinder with a Part-Through Circular Surface Flaw - Compliance Calibration and Collocation Method		5. TYPE OF REPORT & PERIOD COVERED Technical report	
7. AUTHOR(s) M. A. Hussain, J. F. Throop, S. L. Pu R. D. Scamlen		8. CONTRACT OR GRANT NUMBER(s)	
9. PERFORMING ORGANIZATION NAME AND ADDRESS Benet Weapons Laboratory Watervliet Arsenal, Watervliet, N.Y. 12189 SARBY-RF-TT		10. PROGRAM ELEMENT, PROJECT, TASK AREA & WORK UNIT NUMBERS AMCMS No. 611102.11.H5400 Proj No. 11161102AH54	
11. CONTROLLING OFFICE NAME AND ADDRESS B. Army Armament Command Rock Island, Illinois 61201		12. REPORT DATE October 1976	
14. MONITORING AGENCY NAME & ADDRESS (if different from Controlling Office) ⑫ 56p. A1		13. NUMBER OF PAGES 54	
		15. SECURITY CLASS. (of this report) UNCLASSIFIED	
		15a. DECLASSIFICATION/DOWNGRADING SCHEDULE	
16. DISTRIBUTION STATEMENT (of this Report) Approved for public release; distribution unlimited.			
17. DISTRIBUTION STATEMENT (of the abstract entered in Block 20, if different from Report)			
18. SUPPLEMENTARY NOTES			
19. KEY WORDS (Continue on reverse side if necessary and identify by block number) Fracture Mechanics      Compliance Surface Flaw              Stress Intensity Factor Collocation			
20. ABSTRACT (Continue on reverse side if necessary and identify by block number) The K calibration at the deepest point of a circular surface flaw in an internally pressurized thick-walled cylinder has been determined by a compliance test as well as a three-dimensional collocation method. Compliance is defined as the change in the internal volume of a cylinder divided by an applied hydrostatic pressure instead of the usual elongation/load definition. It is shown, using the linear theory of elasticity that the derivative with respect to the crack depth of internal and external volume changes are → next page (See Other Side)			

20.

identical. This permits the use of external strain measurements to compute the stress intensity factors. Periodic cubic splines are used to interpolate/ approximate the strain data as well as to compute external volume change as a function of crack depth. The results agree very well with theoretical results obtained by the three-dimensional collocation method.



Accession No. [ ]  
ATIS [ ]  
DOC [ ]  
UNCLASSIFIED [ ]  
JUSTIFICATION [ ]  
SP [ ]  
LISTED IN [ ]  
Dis. [ ]  
A

## TABLE OF CONTENTS

	<u>Page</u>
REPORT DOCUMENTATION PAGE DD FORM 1473	
INTRODUCTION	1
ANALYSIS OF COMPLIANCE CALIBRATION, SECTION 1 -	3
COMPLIANCE TEST, SECTION 2 -	7
DATA ANALYSIS, SECTION 3 -	13
RESULTS BY COLLOCATION METHOD, SECTION 4 -	23
CONCLUDING REMARKS	45
REFERENCES	46
APPENDIX	47

## ILLUSTRATIONS

1. Cross sections showing a surface flaw in a gun tube.	2
2. Schematic diagram showing the specimen for compliance test.	6
3. The final fracture surface of a Fatigue Test Specimen.	11
4. Crack profiles at successive crack depths.	12
5. Figures indicating the smooth nature of the strain data and interpolating splines.	
a. Strain data for crack depth of 0.50 in.	16
b. Strain data for crack depth of 0.75 in.	17
c. Strain data for crack depth of 1.00 in.	18
d. Strain data for crack depth of 1.50 in.	19
e. Strain data for crack depth of 2.00 in.	20

	<u>Page</u>
6. Comparison of stress intensity factors with ( $h=1$ ) and without ( $h=0$ ) Irwin correction for pressures at 40 and 48 ksi.	22
7. The stress intensity factors as functions of crack depth for sequential pressure levels with $h=0$ .	
a. Pressure increased to 32 ksi.	24
b. Pressure increased to 48 ksi.	25
c. Pressure decreased to 40 ksi.	26
d. Pressure decreased to 32 ksi.	27
8. The stress intensity factors as functions of crack depth for sequential pressure levels with $h=0.2$ .	
a. Pressure increased to 32 ksi.	28
b. Pressure increased to 48 ksi.	29
c. Pressure decreased to 40 ksi.	30
d. Pressure decreased to 32 ksi.	31
9. The stress intensity factors as functions of crack depth for sequential pressure levels with $h=1.0$ .	
a. Pressure increased to 32 ksi.	32
b. Pressure increased to 48 ksi.	33
c. Pressure decreased to 40 ksi.	34
d. Pressure decreased to 32 ksi.	35
10. A rectangular block with a circular surface flaw is used to simulate a shallow surface crack in a thick-walled tube.	36
11. Graph of $K_I/p$ vs $N$ showing the stability of collocation results for $N>15$ .	42
12. Graph of $K_I/p$ vs $\theta$ for $N=28$ with 109 collocation points.	43

	<u>Page</u>
13. Graph of $K_I/p$ vs. $b$ , obtained by compliance tests and collocation method for non-autofrettage tube.	44
A1. Graph of $K_I/p$ vs. $b$ for 30% autofrettaged tube.	48

TABLES

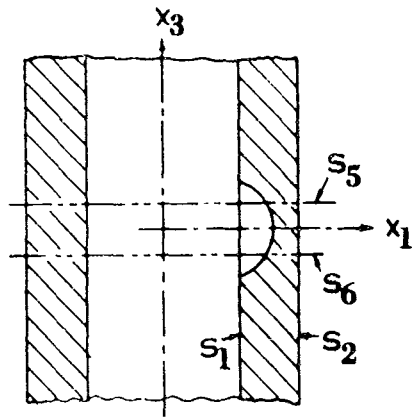
1. Circumferential strains (in./in. $\times 10^6$ ) at 48,000 psi pressure for the successive crack depths (in.).	8
2. Change in area $\Delta A_0$ (in <sup>2</sup> ) enclosed by the outer perimeter of the cylinder at $x_2=0$ for various crack depths at sequential pressure levels.	21
3. Values of $A_n$ 's for $N=28$ , $\nu=0.3$ and $a=1$ ", $d=0.3$ ". $TH=5.575$ ", $n_{HW}=3$ ", $HH=3$ " with linear constraint $A_0 = -2A_n \cos n(\cos^{-1}(d/a))$ .	40
A1. Change in cross-section area $\Delta A_0$ (in <sup>2</sup> ) for a 30% autofrettaged tube for various crack depths at sequential pressure levels.	49

## INTRODUCTION

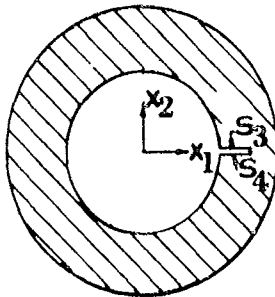
The compliance calibration for two-dimensional cracks is seldom attempted. This is due to the fact that a fairly wide selection of methods (e.g., finite elements, collocation, complex variable, integral equations, etc.) are available to obtain stress intensity factors to a good degree of accuracy and also due to difficulty in performing experiments with sufficient accuracy. For the three-dimensional problems, in general, the difficulties are compounded, analytically as well as experimentally. However, for an internally pressurized thick-wall cylinder with a symmetric internal surface flaw located in the axial direction, the evaluation of compliance can be accomplished. This has been done by proper definition of compliance and data reduction. In fact, a fatigue crack originating at the bore surface tends to be orientated with its length in the axial direction and depth in the radial direction.

The theoretical basis for the compliance test using the linear theory of elasticity is given in Section one.

With a starter notch of a semi-circular cross-section an extensive set of tests were performed as explained in Section two. In the third section, the method of numerical data analysis is outlined, and the stress intensity factors are computed. In Section four, we simulate the actual crack by a simpler geometry and using the method of three-dimensional collocation, the stress intensity factors are computed. The experimental results compare well with the theoretical results obtained. To the authors' knowledge, such a  $K_I$  calibration does not exist in the literature.



SECTION  $x_2 = 0$



SECTION  $x_3 = 0$

FIGURE 1. Cross sections showing a surface flaw in the gun tube.

## SECTION I - ANALYSIS OF COMPLIANCE CALIBRATION

The volumetric compliance method for a thin, straight-fronted radial notch has been discussed in [1]. For the present problem of a symmetric surface flaw located on an axial plane shown in Figure 1, it is clear that strain energy release rates and stress intensity factors are functions of the axial coordinate  $x_3$ . However, if we restrict our attention to the plane  $x_3=0$  only, the concepts of volumetric compliance can be extended to compute the stress intensity factors at the deepest point of the surface flaw, i.e. at  $x_3=0$ . Let the following quantities be defined at  $x_3=0$ :  $\Delta V_i$  is the change in the internal volume per unit length in  $x_3$ , due to the internal pressure  $p$ ;  $G$  is the crack extension force (strain energy release rate);  $C_v = \Delta V_i/p$  is the volumetric compliance, and  $b$  is the crack depth. Then,

$$G = \frac{1}{2} p^2 \frac{dC_v}{db} \quad , \quad \text{at } x_3=0 \quad , \quad (1)$$

The stress intensity factor at  $x_3=0$ , denoted by  $K_1$  is,

$$K_1^2 = \frac{E}{(1-\nu^2)} G = \frac{E p^2}{2(1-\nu^2)} \frac{d}{db} (\Delta V_i/p) \quad , \quad \text{at } x_3=0 \quad . \quad (2)$$

The above relation is a consequence of a 'plane strain' condition at  $x_3=0$ , [2]. As indicated in (2), the compliance calibration can be

<sup>1</sup>UNDERWOOD, J.H., LASSELLE, R.R., SCANLON, R.D. and HUSSAIN, M.A., "A Compliance K Calibration For A Pressurized Thick-Wall Cylinder With A Radial Crack" Engineering Fracture Mechanics, Vol. 4, 1976, pp. 231-244.

<sup>2</sup>EMERY, A.F. and SMITH, F.W., "Some Basic Properties of Penny-Shaped Cracks" Mathematika, Vol. 13, 1966, pp. 172-180.

accomplished at a given value of pressure by determining the change in the internal volume of the cylinder (at  $x_3=0$ ) for a series of surface flaws of different depths and performing the indicated differentiation. However, the measurement which can easily be made is the change in the outside volume of the cylinder per unit length at  $x_3=0$  (equivalent to the change in cross-sectional area at  $x_3=0$ ). In the sequel we will prove that the derivative of internal and external volume changes for a given pressure is identical.  $\Delta V_0$  and  $\Delta V_m$  are the changes in the outside volume and material volume per unit length at  $x_3=0$ . Hence

$$\Delta V_0 = \Delta V_i + \Delta V_m \quad (3)$$

If  $\delta V$  is the total change in the material volume  $V$  bounded by cylindrical surfaces  $S_1$  and  $S_2$  between cross-sections  $S_5: x_3=l$  and  $S_6: x_3=-l$  and exterior to the upper and lower surfaces of the surface flaw  $S_3$  and  $S_4$ , Figure 1, we have

$$\delta V = \int_V e \, dV \quad (4)$$

where  $e = e_{11} + e_{22} + e_{33}$  is the dilation. The generalized Hooke's law for a homogeneous isotropic body can be written (using the usual notations) in the following form: (see e.g. [3])

$$\tau_{ij} = \lambda \delta_{ij} e + 2\mu e_{ij} \quad , \quad (i, j = 1, 2, 3) \quad (5)$$

Contraction gives:

$$\tau_{ij} = (3\lambda + 2\mu)e \quad (6)$$

Hence

$$\delta V = \frac{1}{3\lambda + 2\mu} \int_V \tau_{ii} \, dV \quad (7)$$

<sup>3</sup>SOKOLNIKOFF, I.S., "Mathematical Theory of Elasticity" McGraw Hill Book Company, New York, 1956, p. 66.

Using the equation of equilibrium

$$\tau_{ik,k} = 0 \quad , \quad (i, k = 1, 2, 3) \quad , \quad (8)$$

one can show:

$$\int_V \tau_{ij} dV = \int_V (\tau_{ik} x_j)_{,k} dV \quad . \quad (9)$$

The divergence theorem yields

$$\int_V (\tau_{ik} x_j)_{,k} dV = \int_S \nu_k \tau_{ik} x_j dS = \int_S \overset{\nu}{T}_i x_j dS \quad (10)$$

where  $S$  is a surface forming the complete boundary of the volume  $V$  and  $\nu_i$  are the direction cosines of the outer normal  $\nu$  of  $S$  and  $\overset{\nu}{T}_i$  are the components of the traction  $\overset{\nu}{T}$  acting on  $S$ . Hence we have from (9) and (10)

$$\int_V \tau_{ij} dV = \int_S \overset{\nu}{T}_i x_j dS \quad (11)$$

and contraction gives

$$\int_V \tau_{ii} dV = \int_S \overset{\nu}{T}_i x_i dS = \int_S \overset{\nu}{T} \cdot r dS \quad (12)$$

The surface  $S$  in Figure 1 is formed by six surfaces denoted by  $S_1, S_2, \dots, S_6$  then

$$\Delta V_m = \frac{\Delta V}{2\epsilon} = \frac{i}{2\epsilon} \frac{i}{3\lambda + 2\mu} \sum_{n=1}^6 \int_{S_n} (\overset{\nu}{T})_n \cdot r dS \quad (13)$$

where  $(\overset{\nu}{T})_n$  are tractions on the surface  $S_n$ . From the symmetry we have  $(\overset{\nu}{T})_3 = (\overset{\nu}{T})_4$  and  $(\overset{\nu}{T})_5 = (\overset{\nu}{T})_6$  and the outer normals are in opposite directions for each pair  $(S_3, S_4)$  and  $(S_5, S_6)$ . The last four integrals, having possibly the crack depth  $b$  as a parameter, vanish. This completes the proof that  $\Delta V_m$  is independent of  $b$ .

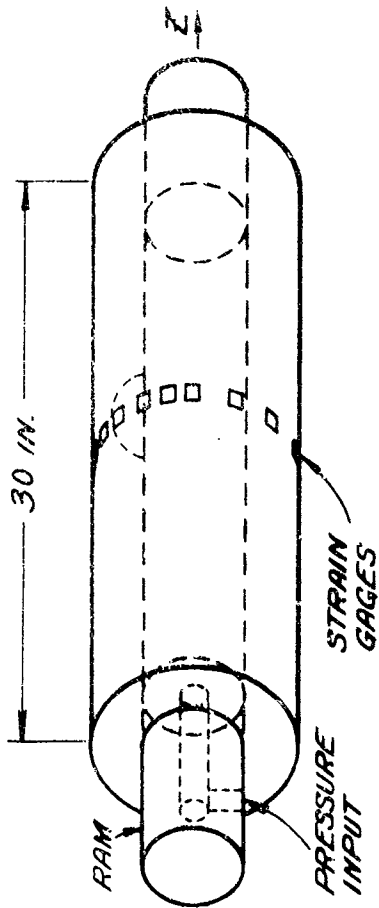


FIGURE 2. Schematic diagram showing the specimen for compliance test.

For an internally pressurized cylinder we have  $(T)_1^v = -e_r p$ ,  $(T)_2^v = 0$ , where  $e_r$  is a unit vector in the radial direction. Thus

$$\Delta V_0 = \frac{1}{3} \frac{1}{2} 2\pi p r_1^2 \quad (14)$$

and from (3)

$$\frac{d(\Delta V_0)}{db} = \frac{d(\Delta V_1)}{db} \quad (15)$$

The stress intensity factor then can be written in terms of the outside volume change of the cylinder per unit length

$$K_{I,0}^v = \left[ \frac{E}{2(1-\nu^2)} \frac{d(\Delta V_0/p)}{db} \right]^{1/2} \text{ at } x_3=0 \quad (16)$$

#### SECTION 2. EXPERIMENTAL TEST

The specimen, made from a steel cannon tube, was a cylinder with a 7.1 inch smooth bore and a 14.25 inch outside diameter, giving a diameter ratio of 2.007 and a wall thickness of 3.575 inches. The length was 30 inches with a recess 1.5 inch long and 7.3 inch diameter at each end for the pressure seal.

It was tested as a vertical, hollow cylinder, internally pressurized on a supporting mandrel so that the end loads were supported by the internal mandrel, giving an open end condition. (See Figure 2.) The cylinder ends were sealed with threaded closures on the mandrel so that there were no axial stresses produced in the specimen due to pressure end loads. The pressure fluid was a synthetic instrument oil which remains fluid at pressures in excess of those used. The pressure was fully exerted in the initial notch cavity when the cylinder was pressurized.

Table 1. Circumferential Strains (in./in. x 10<sup>6</sup>) at 43,000 psi Pressure for the Successive Crack Depths (in.)

GAGE LOCATION (DEGREE)	CRACK DEPTH AND THE CORRESPONDING NO. OF CYCLES TO REACH THE DEPTH									
	0.25	0.50	0.75	1.0	1.5	2.0	2.5	3.15	3.975	
	0	4600	5450	6760	8700	9750	10200	10550		
-180	1105	1085	1090	1120	1060	1035	920	950	950	Not
-135	1095	1095	1100	1105	1070	1055	-	-	-	
- 90	1105	1095	1100	1135	1115	1135	-	-	-	Taken
- 60	1105	1095	1100	1150	1160	1230	-	-	-	
- 30	1105	1115	1135	1190	1295	1510	-	-	-	
- 15	1105	1095	1105	1155	1255	1620	2280	3000	3000	Due
- 5	1110	1050	1045	1040	930	885	-	-	-	
0	1060	1060	1045	1030	865	675	360	490	490	
0	1095	1060	1045	1030	860	665	360	510	510	
5	1110	1065	1050	1050	960	1035	-	-	-	
15	1090	1085	1090	1135	1255	1660	2280	2840	2840	To
30	1100	1110	1120	1185	1315	1520	-	-	-	
60	1095	1105	1120	1140	1160	1225	-	-	-	
90	1100	1105	1100	1125	1110	1120	-	-	-	
135	1095	1085	1095	1110	1060	1050	-	-	-	
180	1105	1085	1090	1120	1060	1035	920	950	950	Failure

The wall was initially notched with a semi-circle of 1/4 inch radius cut at the bore by electrical discharge machining (EDM). The notch was 1/2 inch long in the axial direction, 1/4 inch deep in the radial direction and 0.030 inch wide in the circumferential direction at the midsection of the specimen. A fatigue crack was grown from this starter notch by hydraulic pressure cycling from zero to 48,000 psi until it reached each successive desired depth, as determined by ultrasonic crack-depth measurement. The circumferential strains were then read on the outside circumference with bonded foil strain gages at 14 angular positions relative to the notch location.

The strain gages were 1/4 inch gage length and were oriented in the circumferential direction in a ring at specimen midlength. Two gages were located on a line directly over the notch, one at 1 inch above and one at 1 inch below the cylinder midlength, so as to permit measurement of crack depth at its deepest point by placement of an ultrasonic normal probe directly over the notch. Other gages were located around the midlength circumference at angles from  $5^{\circ}$  to  $180^{\circ}$  on either side of the notch line, as listed in Table 1.

When measuring the strains at each crack depth, the pressure was increased to 16000, 32000 and 48000 psi and then decreased to 40000, 32000, 24000, 16000, 8000, 4000 and zero. The pressures were controlled within  $\pm 1\%$ . The readings from all gages were taken in sequence, with the cylinder held at pressure, using a 24 channel switching unit and an SR-4 strain indicator located outside the test cell. An identical strain gage, bonded to an unstrained piece of the same steel lying on the

test specimen provided temperature compensation during the experiments. If the final strain reading at zero pressure differed from the initial zero pressure reading by more than 20 microinches per inch at any crack depth the readings were repeated to eliminate measurement errors as much as possible.

Strain gage data for the 48000 psi pressure level are listed for the successive crack depths in Table 1. The gage positions are the angular locations on the O.D. from a point directly over the initial notch.

Figure 3 shows the final fracture surface of this fatigue crack.

The crack profile at successive crack depths is reproduced in Figure 4. The corresponding number of cycles to reach each depth is given in Table 1. Figures 3 and 4 show that the crack, propagated from the initial semi-circular notch, remained a semi-circle until nearly 2-inch depth was reached. After that it became part-circular or part-elliptical. It finally acquired the shape of a partially imbedded ellipse, when the intersection of the crack front with the bore surface became nearly stationary while the ellipse deepened and lengthened. In these latter stages of growth, after a 2-in. depth, the rate of propagation was quite fast. Unfortunately we did not obtain as complete strain data as would be required for an accurate compliance analysis for the greater depths. The data is therefore analyzed for the semi-circular shape up to the 2-inch depth only. In Figure 3 one can see the evidence of a "free surface shear-lip" formation which fans out at about  $20^{\circ}$  from the inner wall on either side of the initial notch.



FIGURE 3. The final fracture surface of a Fatigue Test Specimen.

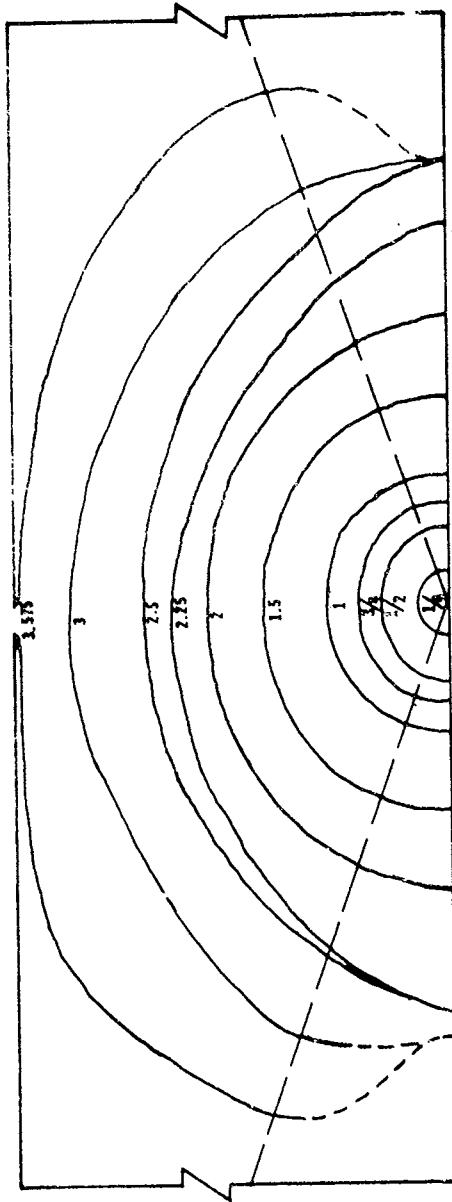


FIGURE 4. Crack profiles at successive crack depths.

### SECTION 3 - DATA ANALYSIS

by considering only the cross-section of the cylinder through the strain gages (i.e.,  $x_3=0$ ) the numerical problem is stated as follows. Given the tangential strain at selected points on the circumference of a circle, we wish to determine numerically the change in cross-sectional area (equivalently  $\Delta V_0$ , the change in external volume per unit length at  $x_3=0$ ).

This can be accomplished in two ways. First, we can integrate the tangential strain to obtain the change in the length of the perimeter

$$\Delta P = \int_0^{2\pi} r_2 \epsilon_\phi(\phi) d\phi, \quad \text{at } x_3=0, \quad (17)$$

and assuming the distorted figure remains circular, we have the change in cross-section area  $\Delta A_0$ :

$$\Delta A_0 = \frac{1}{4\pi} (2P\Delta P + \Delta P^2). \quad (18)$$

A more rigorous approach is to compute

$$\Delta A_0 = \int_0^{2\pi} \int_{r_2}^{r_2+u_r(r,\phi)} r dr d\phi \quad (19)$$

From strain displacement relations, we have (using cylindrical coordinates):

$$u_r(r_2, \phi) = r_2 \epsilon_\phi(r_2, \phi) - \frac{\partial u_\phi(r_2, \phi)}{\partial \phi}, \quad (20)$$

where  $u_r$ ,  $u_\phi$  are radial and tangential displacements. It can be shown by eigenfunction expansions that the second term at the right of (20), for the present problem, is even in  $\phi$  and periodic in  $2\pi$ . Neglecting second order terms (linear elasticity), it is seen that this term makes no contribution to the integral in (19). Hence, essentially

we have  $u_r(r_2, \phi) \equiv r_2 \varepsilon_\phi(r_2, \phi)$  for the integration of (19). It was found that the evaluations of  $\Delta A_0$ , using the two methods, agree with each other to four significant figures.

For the data analysis, our choice of an angular function was an interpolating periodic cubic spline [4].

Definition of cubic spline:

$$\text{Given an interval, } \alpha \leq x \leq \beta, \quad (21)$$

a mesh on the interval,

$$\Delta: \alpha = x_0 < x_1 < \dots < x_N = \beta, \quad (22)$$

and associated set of ordinates (data points),

$$Y: y_0, y_1, \dots, y_N \quad (23)$$

then the cubic spline satisfies:

$$\begin{aligned} S_\Delta(Y; x) &\in C^2 \text{ on } [\alpha, \beta], \\ S_\Delta(Y, x_j) &= y_j \quad (j=0, 1, \dots, N), \end{aligned} \quad (24)$$

and is coincident with a cubic on each interval,

$$x_{j-1} \leq x \leq x_j \quad (j=1, 2, \dots, N). \quad (25)$$

If, in addition, the derivatives

$$S_\Delta^{(p)}(\alpha+) = S_\Delta^{(p)}(\beta-) \quad (p=0, 1, 2) \quad (26)$$

the spline is said to be periodic with period  $(\beta-\alpha)$ .

If alternatively

$$S_\Delta(Y; x_j) = y_j + \varepsilon_j, \quad (j=0, 1, \dots, N) \quad (27)$$

with the  $\varepsilon_j$  subject to some minimizing constraint; it is said to be an approximating rather than interpolating spline.

<sup>4</sup> AHLBERG, J. H., NILSON, E. N., WALSH, J. L., "The Theory of Splines and Their Applications," Academic Press, New York, 1967.

As described in the previous section the data was taken at 14 angular position for six crack depths and at nine pressures. Discounting the data for crack depths greater than 2 in. (due to gage and tube failures) we have 756 data points for numerical analysis. To indicate the smooth nature of the strain data and interpolating functions we show in Figures 5a - 5e the results for various crack depths at 48,000 p.s.i.

Once the spline function has been found the changes in the cross-sectional area are computed by the methods indicated above. The partial results are presented in Table 2. It should be noted that the first row in Table 2, for zero crack depth, is not empirical data but extrapolated values and the set of data corresponding to starter notch (b-.25) have been eliminated. The stress intensity factors now have to be computed from (16)

$$K_1/p = \left[ \frac{E}{2(1-\nu^2)} \frac{d(\Delta V_0/p)}{db} \right]^{1/2}, \text{ at } x_3=0, \quad (16)$$

where  $\Delta V_0$  is the change in the outside volume of the cylinder per unit length at  $x_3=0$  and thus is numerically equivalent to  $\Delta A_0$  and also from

$$K_1^*/p = \left[ \frac{E}{2(1-\nu^2)} \frac{d(\Delta V_0/p)}{db^*} \right]^{1/2}, \text{ at } x_3=0, \quad (28)$$

where  $b^* = b + \frac{h}{2\pi} \left( \frac{K_1}{\sigma_y} \right)^2$  is an effective crack depth suggested by Irwin [5], ( $0 \leq h \leq 1$ ,  $\sigma_y$  = yield stress) to correct for the effect of plastic deformation at the crack boundary.

<sup>5</sup>IRWIN, G. R., "Structural Aspect of Brittle Fracture", Applied Materials Research, Vol. 3, 65, 1964.

48000 P.S.I.

0.500 IN. CRACK DEPTH

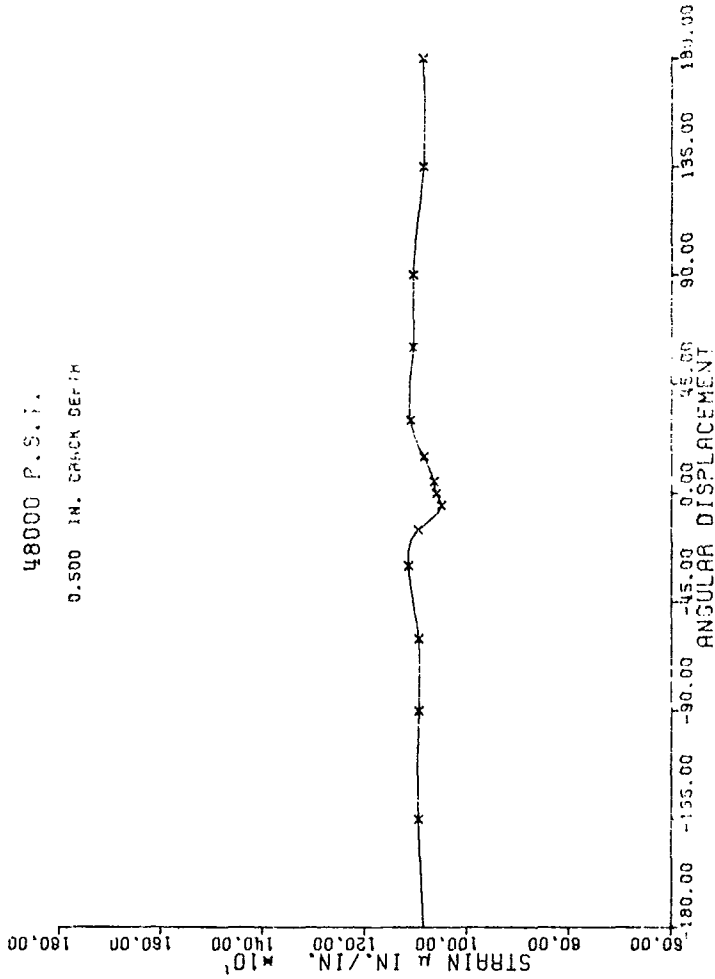


FIGURE 5a. Strain data for crack depth of 0.50 in.

48000 P. S. I.

0.750 IN. CRACK DEPTH

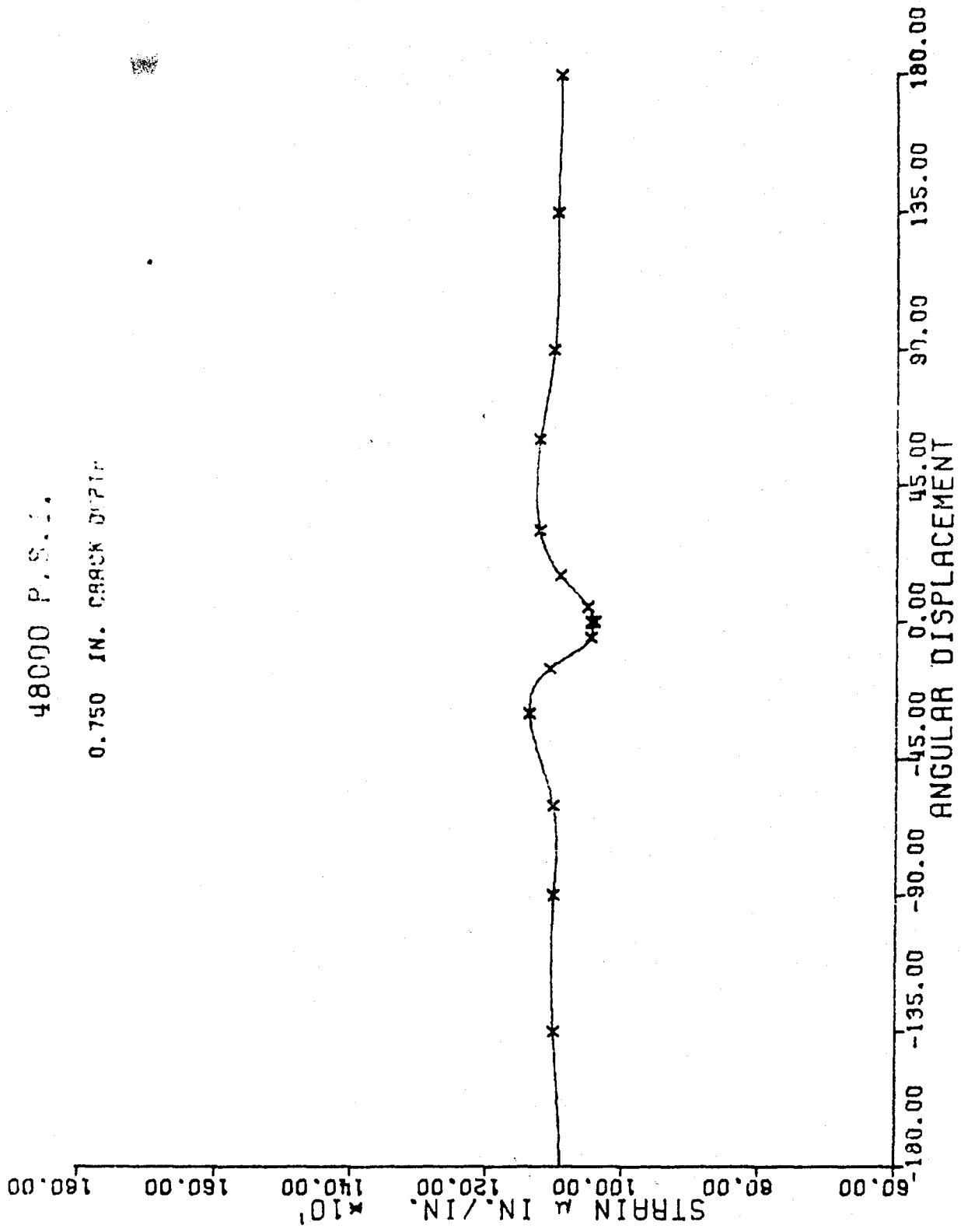


FIGURE 5b. Strain data for crack depth of 0.75 in.

48000 P.S.I.  
1.000 IN. CRACK DEPTH

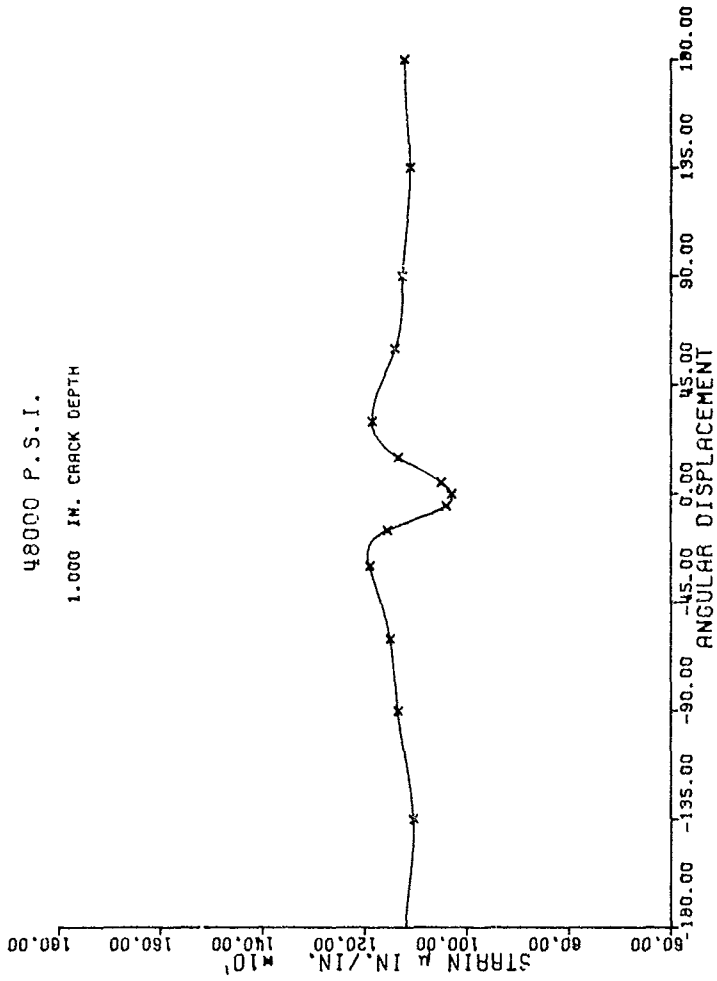


FIGURE 5c. Strain data for crack depth of 1.00 in.

48000 P.S.I.

1.500 IN. CRACK DEPTH

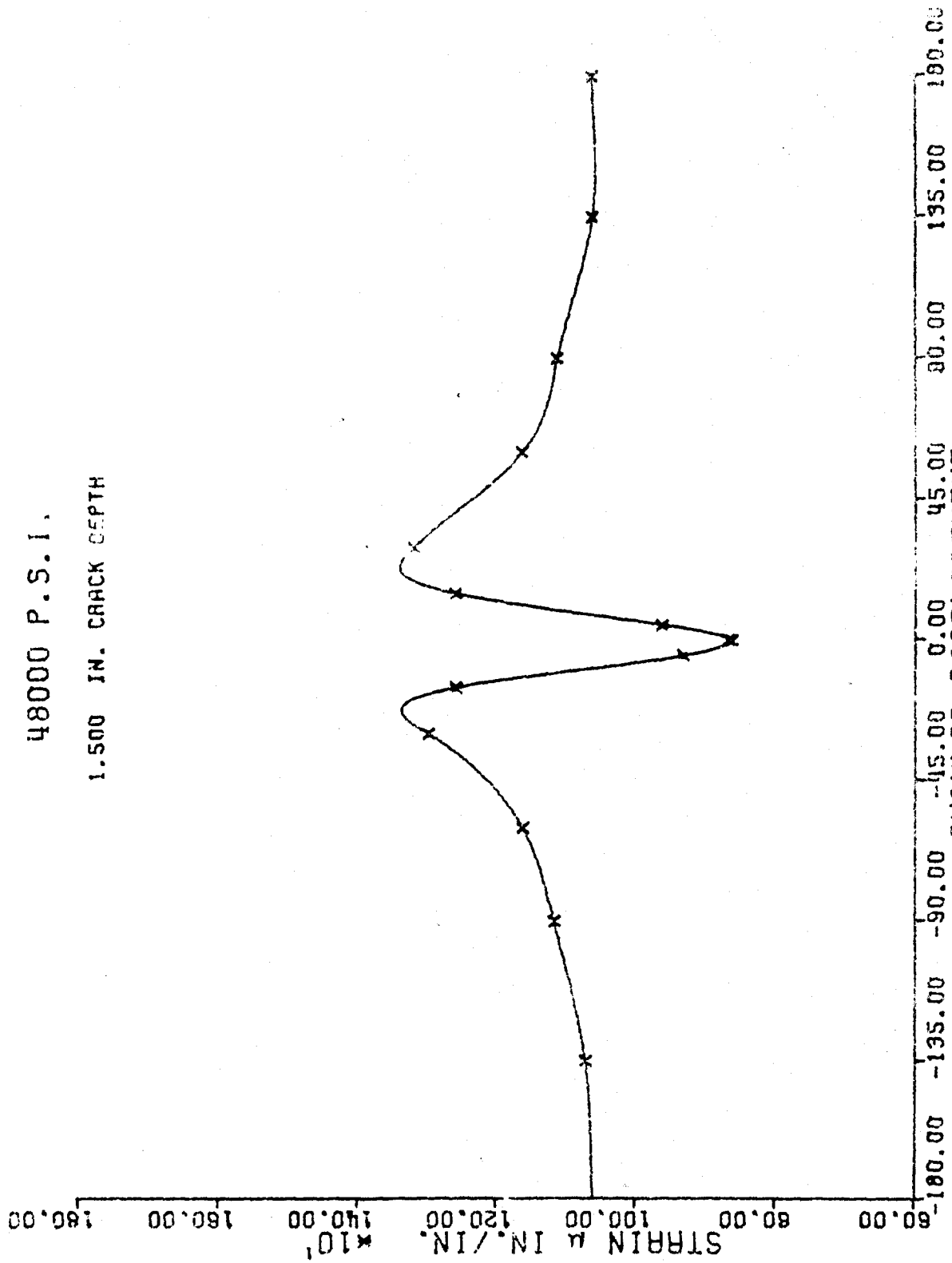


FIGURE 5d. Strain data for crack depth of 1.50 in.

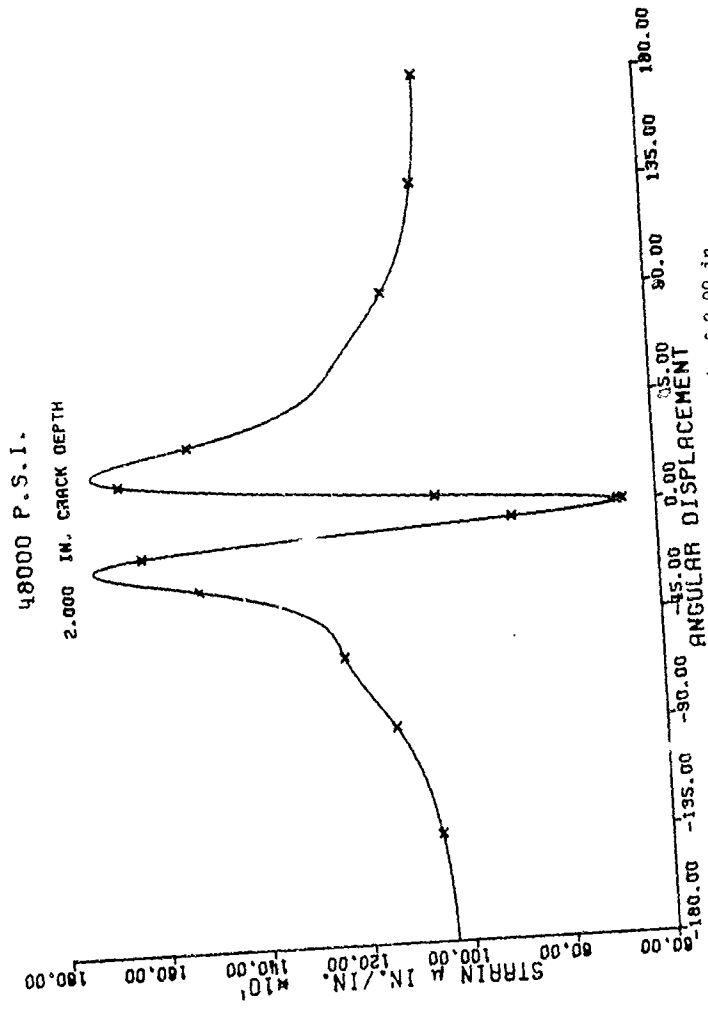


FIGURE 5e. Strain data for crack depth of 2.00 in.

Table 2. Change in Area  $\Delta A_0$  (in<sup>2</sup>) Enclosed by the Outer Perimeter of the Cylinder at  $x_3 = 0$  for Various Crack Depths at Sequential Pressure Levels

CRACK DEPTH b in	PRESSURE p psi			
	32,000	48,000	40,000	32,000
0	0.2312	0.3468	0.2890	0.2312
0.5	0.2325	0.3493	0.2908	0.2328
0.75	0.2326	0.3512	0.2911	0.2334
1.0	0.2375	0.3604	0.2958	0.2351
1.5	0.2389	0.3591	0.2989	0.2392
2.0	0.2496	0.3767	0.3142	0.2507

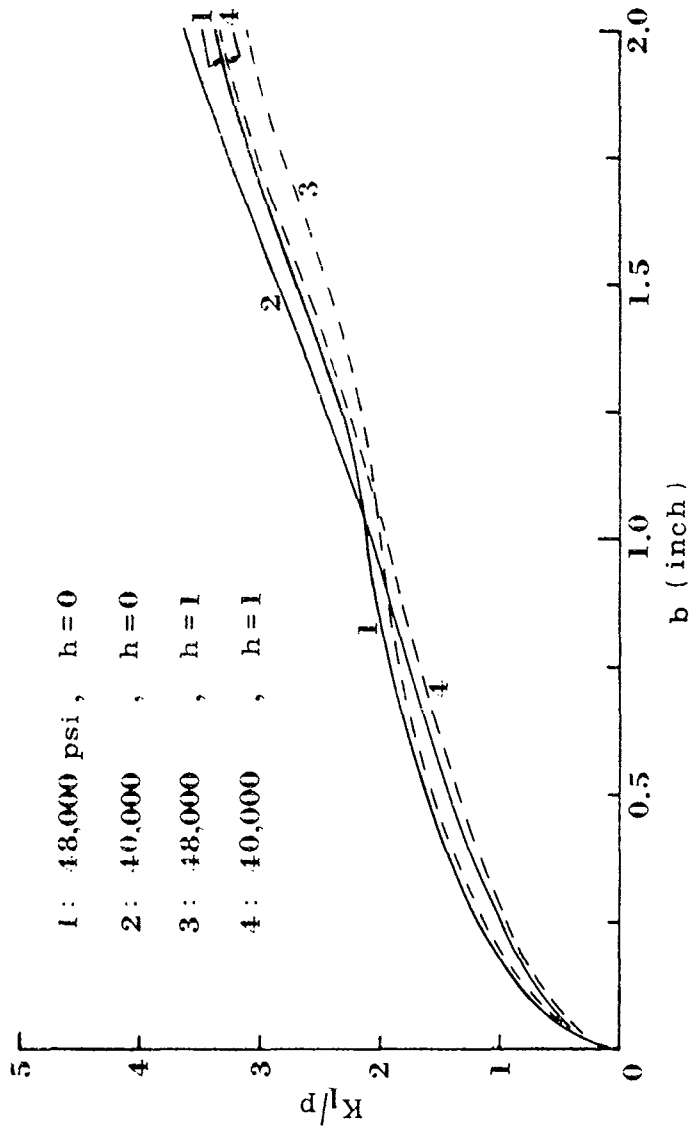


FIGURE 6. Comparison of stress intensity factors with ( $h=1$ ) and without ( $h=0$ ) Irwin correction for pressures at 40 and 48 ksi.

To compute the derivative of  $\Delta V_0(b)$  we used a non-periodic approximating cubic spline with an algorithm which minimized

$$\int_0^{b_n} \{S''_{\Delta}(b)\}^2 db + \lambda \sum_{i=1}^n \{S_{\Delta}(b_i) - \Delta V_{0i}\}^2 \quad (29)$$

where  $\lambda$  is introduced to allow us to strike a balance between the amount of smoothing desired vs. maintaining the integrity of data. As seen from (28) we must of necessity evaluate  $b^*$  and  $K_1^*/p$ , for a given value of  $h$ , by an iterative process which is stable. As a guide to selection of  $\lambda$  we consider the type of  $K_1$  expression common in fracture mechanics,  $K_1 = (\text{constant}) b^{1/2}$  and see that  $d^2 K_1 / db^2$  is strictly monotonic increasing. A value of  $\lambda=10$  proved quite reasonable leading to a rapid and stable convergence of  $K_1^*/p$ .

The results of such an analysis for pressures of 40,000 and 48,000 psi are shown in Figure 6. In an ideal linear experiment  $K_1/p$ , for different pressure, should fall on the same curve. To partially account for plastic deformation at the crack surface we have incorporated the Irwin's correction term, as explained before. In Figure 6, we show the results for 48,000 and 40,000 psi without the Irwin-correction ( $h=0$ ) and with correction ( $h=1$ ). For clarity we have deleted the results for intermediate pressures and different values of  $h$ . In Figures 7, 8, and 9 we show the results for different pressures, and  $h$ . In all of these figures it is seen that the results are fairly close to each other.

#### SECTION 4 - RESULTS BY COLLOCATION METHOD

Because of the complexity in the geometry of the problem it seems that an analytic closed-form solution is not yet possible. However,

32000 PSI

LAMBDA = 10

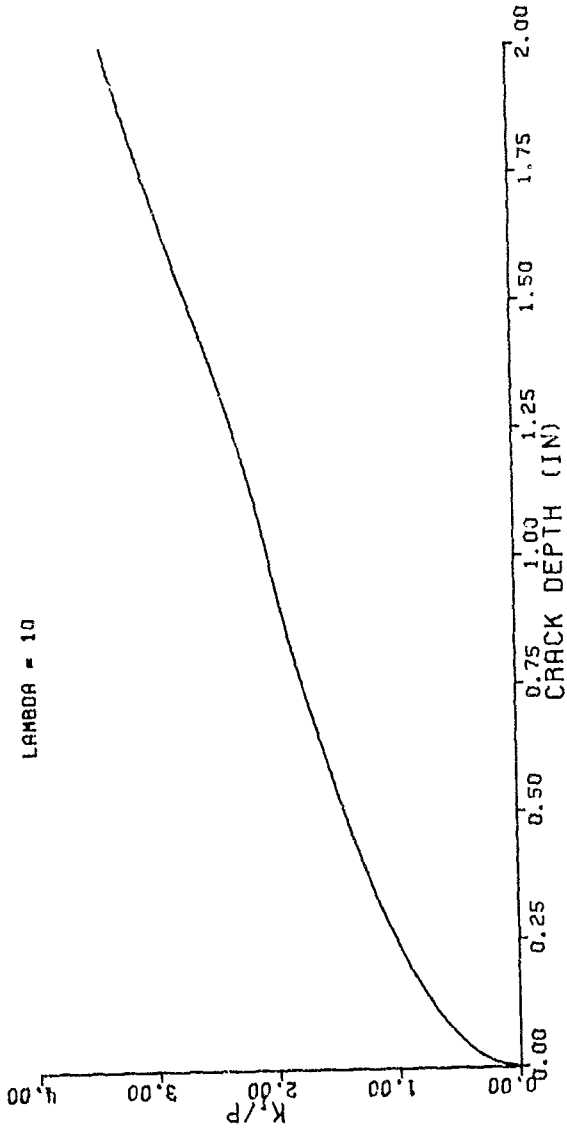


FIGURE 7a. Pressure increased to 32 ksi.

48000 PSI

LAMBDA = 10

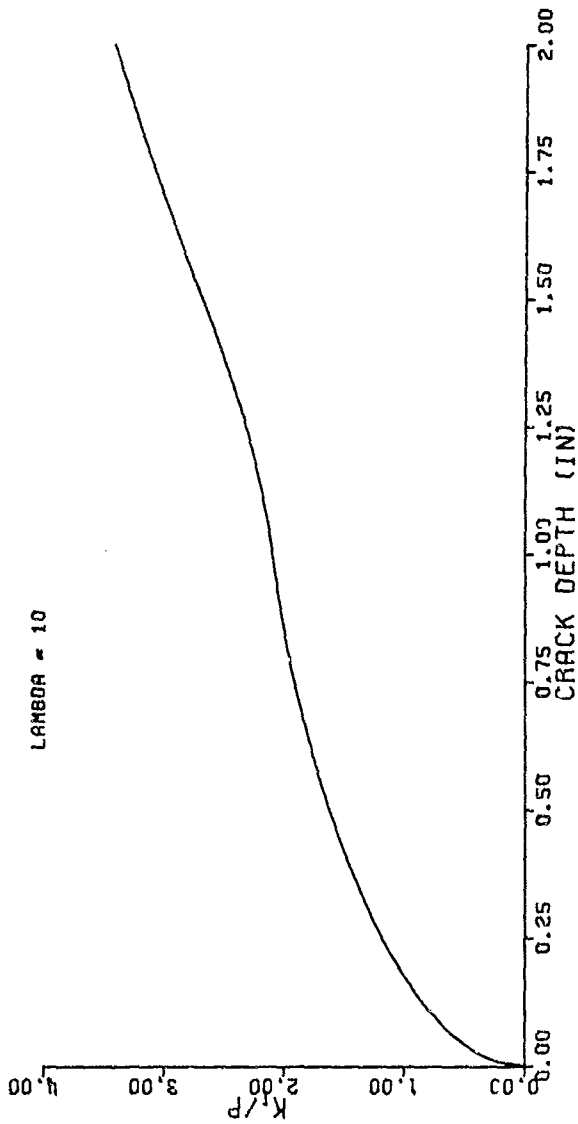


FIGURE 7b. Pressure increased to 48 ksi.

40000 PSI

LAMBDA = 10

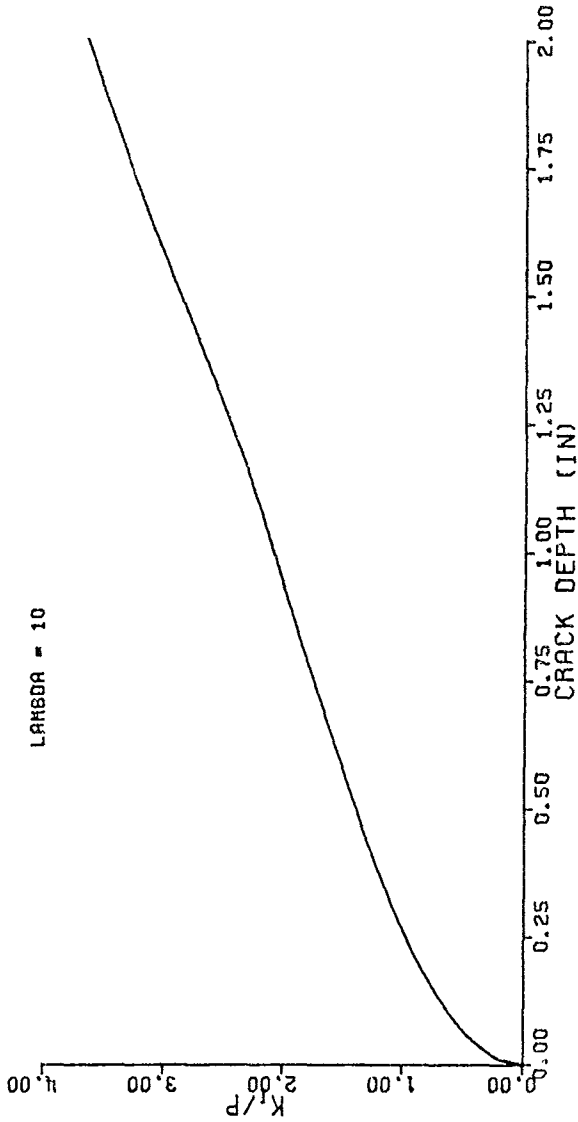


FIGURE 7c. Pressure decreased to 40 ksi.

32000 PSI

LAMBDA = 10

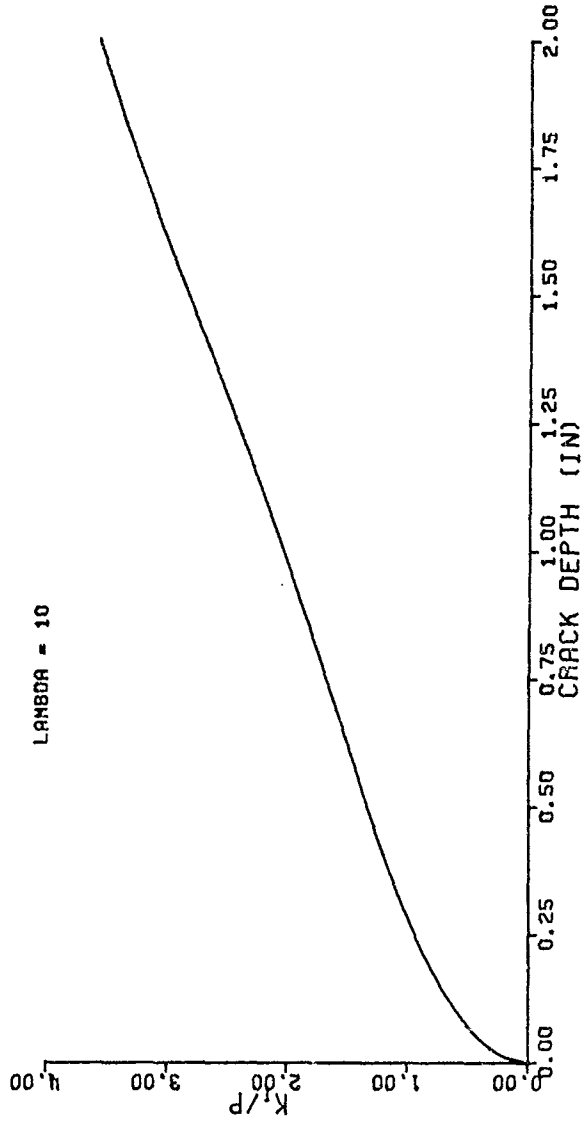


FIGURE 7d. Pressure decreased to 32 ksi.

32000 PSI

LAMBDA = 10

$\mu = 0.20$

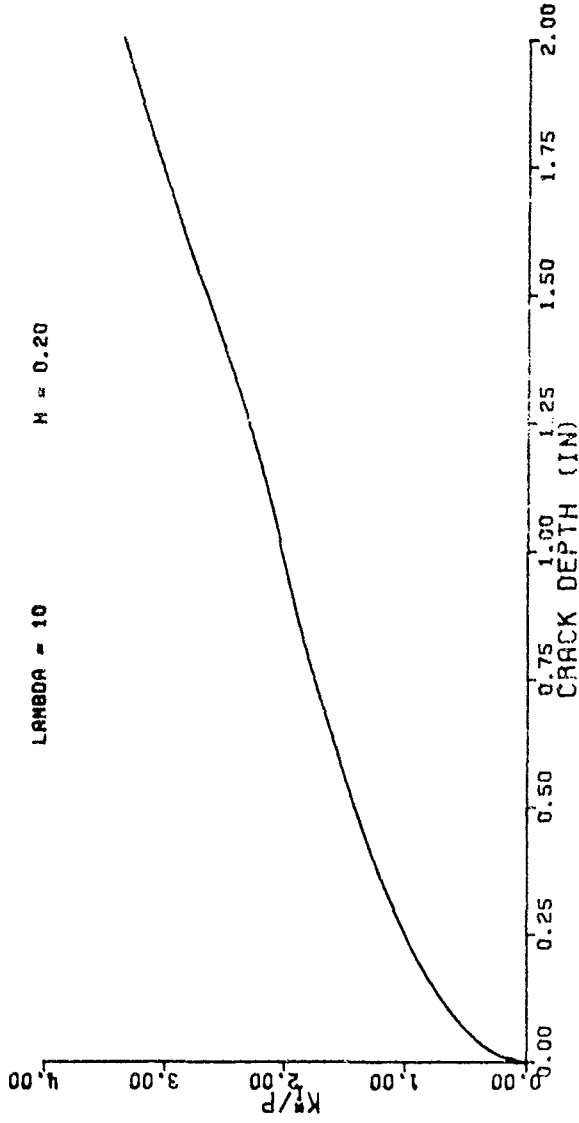


FIGURE 8a. Pressure increased to 32 ksi.

48000 PSI

LAMBDA = 10

H = 0.20

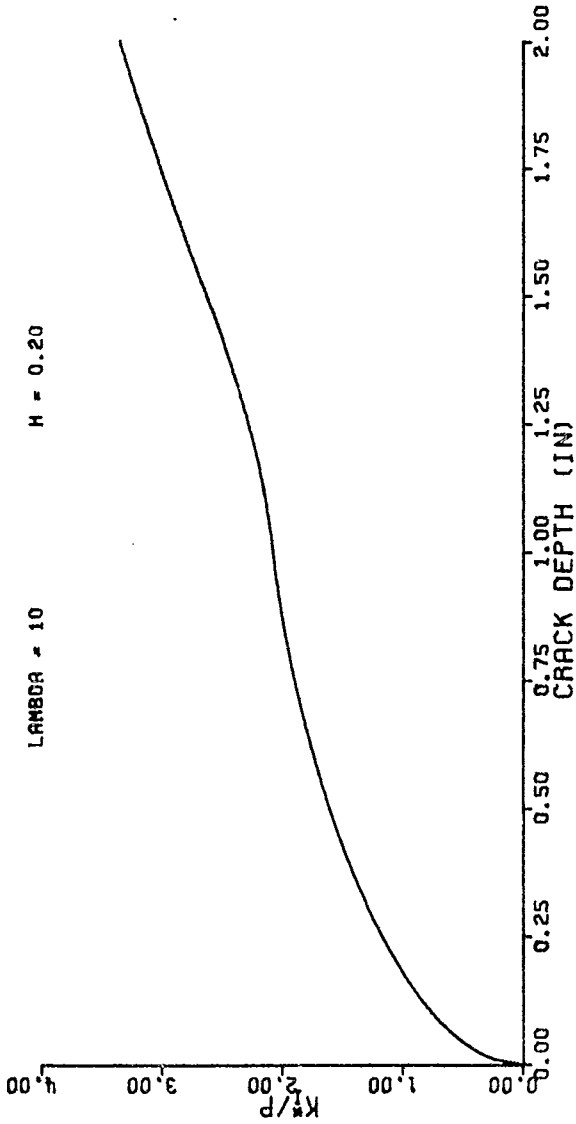


FIGURE 8b. Pressure increased to 48 ksi.

40000 PSI

LAMBDA = 10

R = 0.20

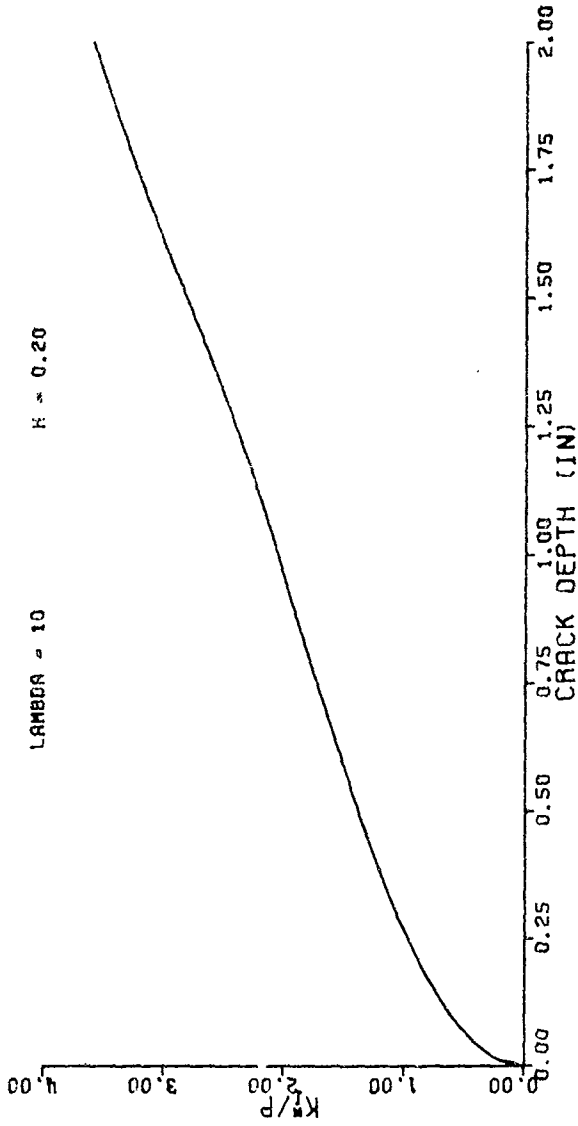


FIGURE 8c. Pressure decreased to 40 ksi.

32000 PSI

LAMBDA = 10

H = 0.20

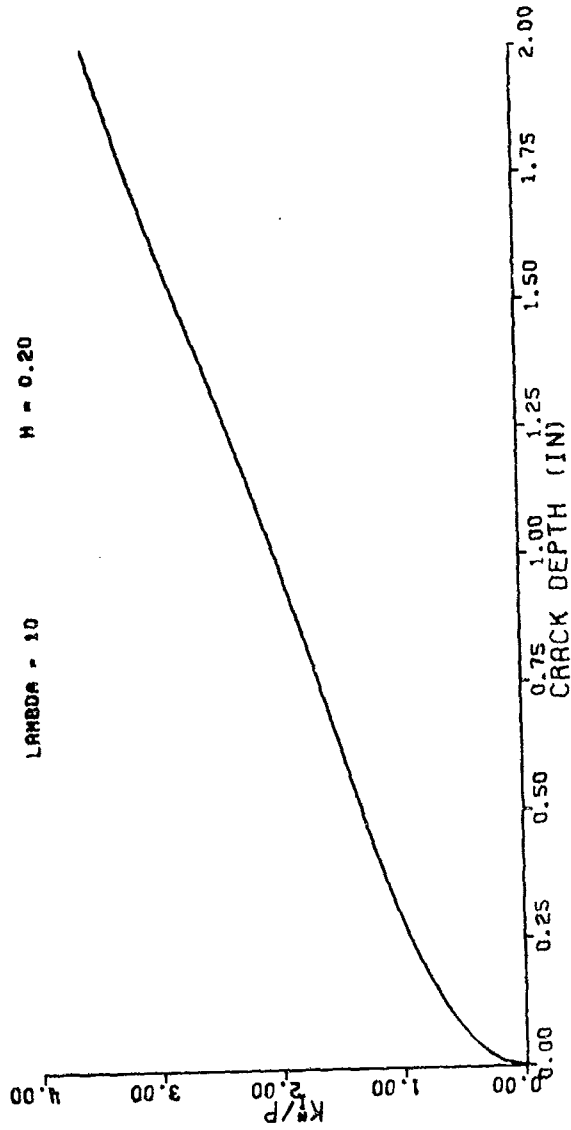


FIGURE 8d. Pressure decreased to 32 ksi.

32000 PSI

LAMBDA = 10

R = 1.00

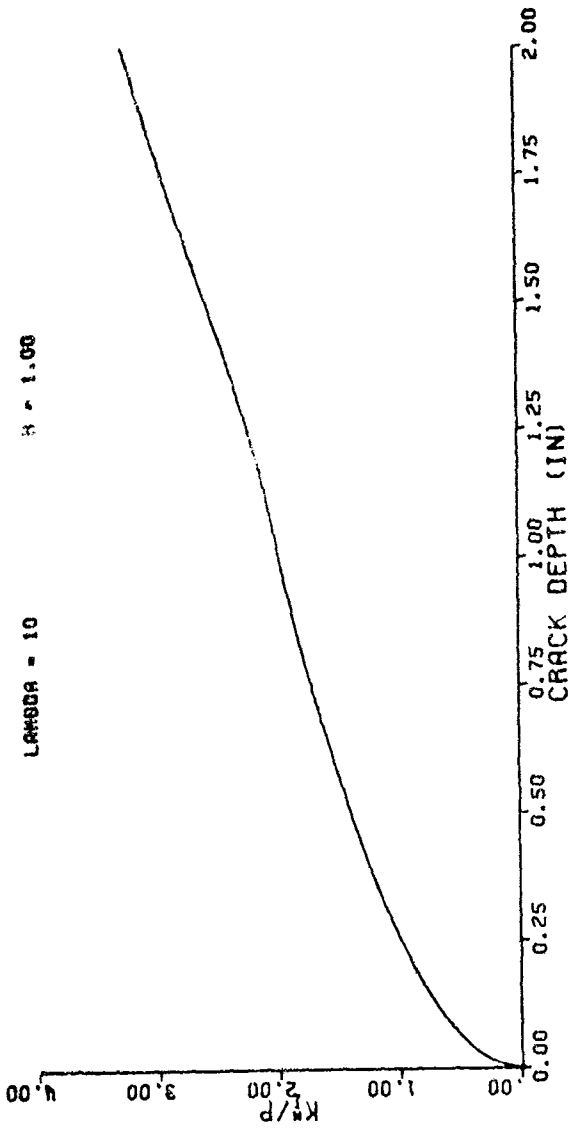


FIGURE 9a. Pressure increased to 32 ksi.

48000 PSI

LAMBDA = 10

H = 1.00

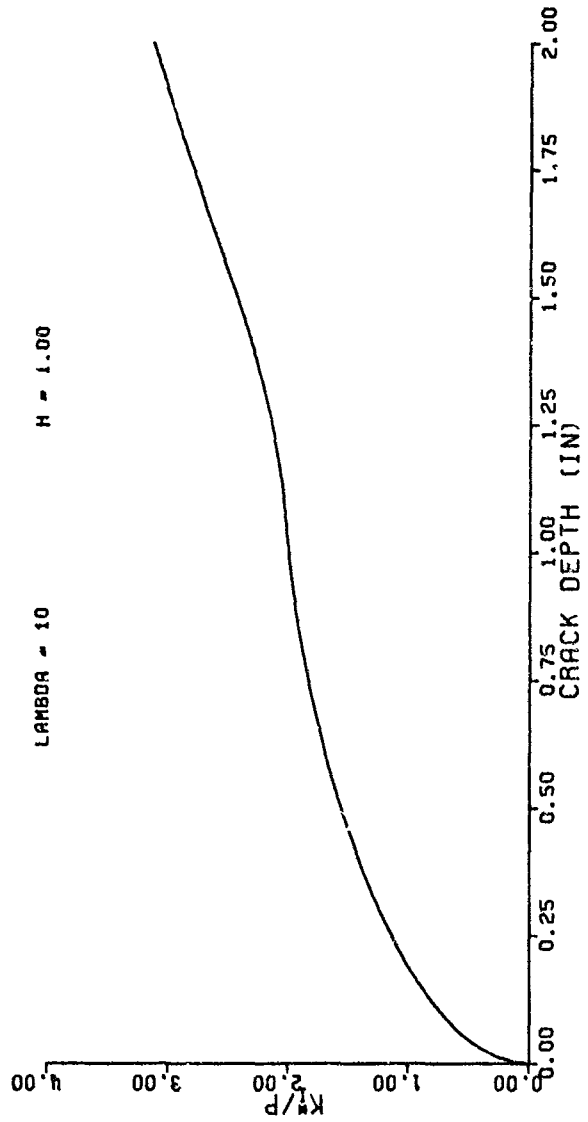


FIGURE 9b. Pressure increased to 48 ksi.

40000 PSI

LAMBDA = 10

H = 1.00

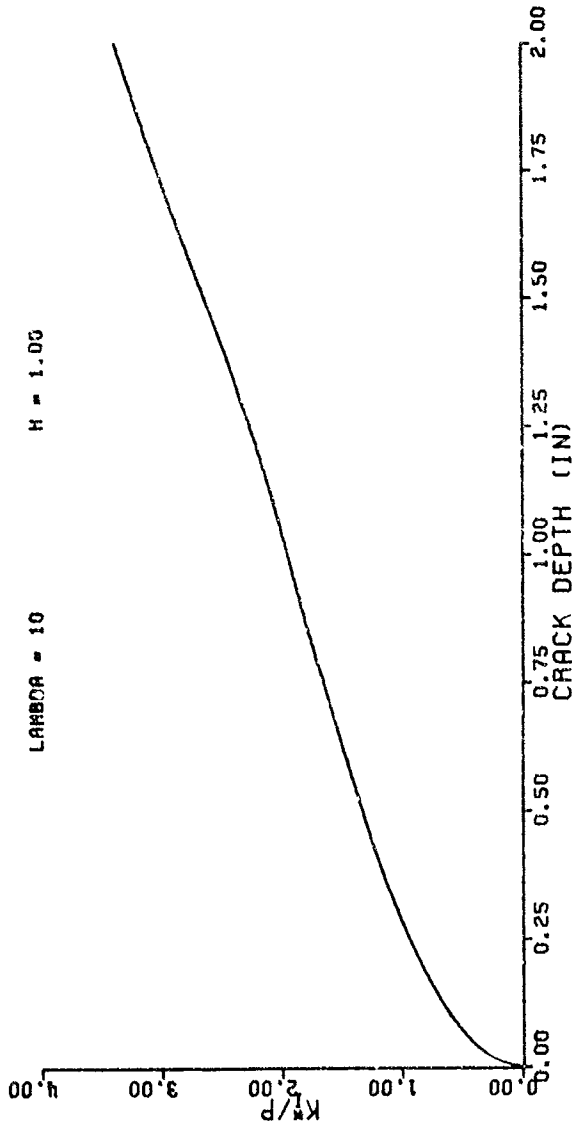


FIGURE 9c. Pressure decreased to 40 ksi.

32000 PSI

LAMBDA = 10

H = 1.00

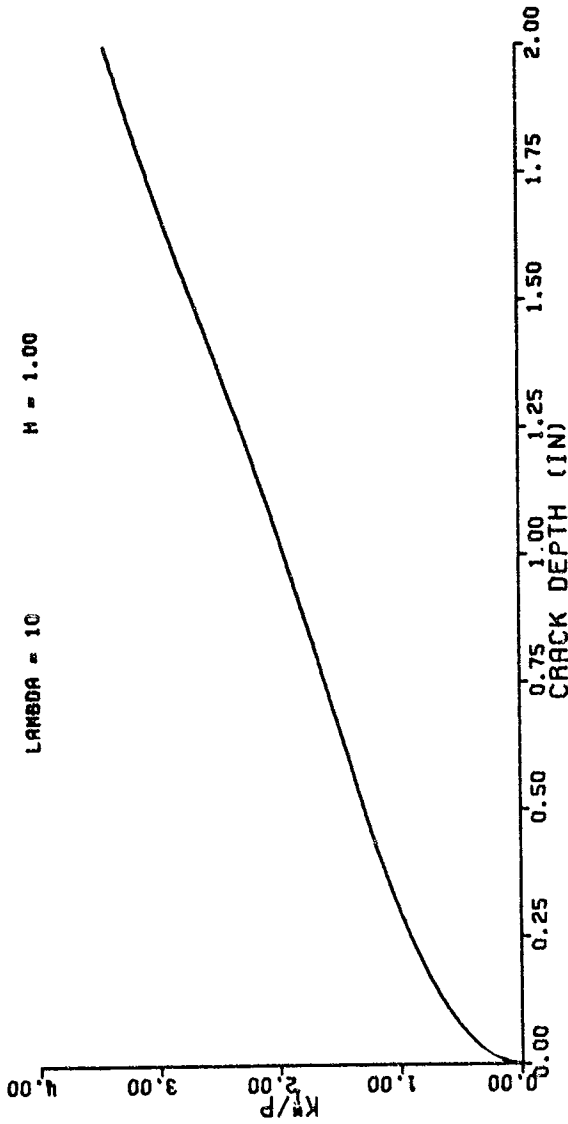


FIGURE 9d. Pressure decreased to 32 ksi.

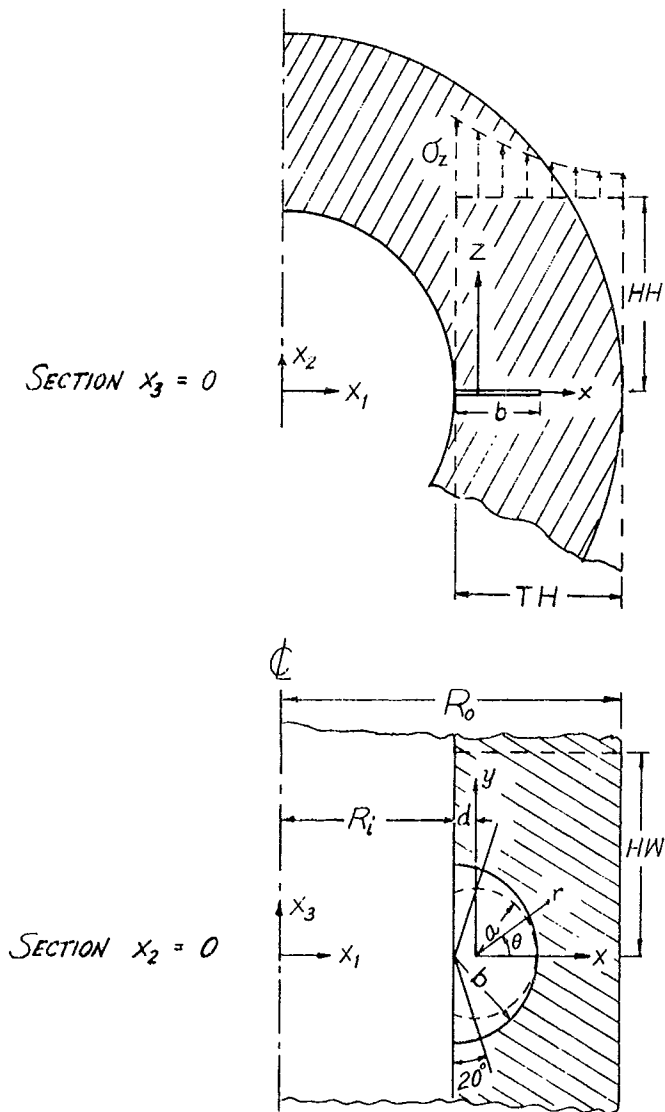


FIGURE 10. A rectangular block with a circular surface flaw is used to simulate a shallow surface crack in a thick-walled tube.

since we are working with relatively shallow surface cracks compared to the wall thickness of the tube (most of the fatigue life is confined to such crack growth as seen from Table 1) we can effectively simulate the curved surface of the tube by a rectangular block with a surface flaw in the form of a segment of a circle as shown in Figure 10 and apply the method of collocation. It is evident from Figures 3 and 4 that there is a 'shear lip' region extending radially to about  $20^\circ$  on either side of the inner wall of the tube. Hence the actual crack was simulated by a segment of a circle with a matching depth and the center having an offset  $d$  of  $.3(\text{radius})$  of the circle as shown, i.e.  $(b=a+d)$ . The thickness (TH) of the block was taken equal to the wall thickness (i.e.  $TH=R_0-R_i$ ) and it was found that it is sufficient to take half the width (HW) and half the height (HH) equal to three times the radius of the crack ( $HW=HH=3a$ ). The loading condition on the block corresponds to the Lamé solution together with uniform tension due to the presence of pressure inside the crack:

$$\sigma_z/p = 1 + \frac{1}{1 - \frac{R_i^2}{R_0^2}} \left\{ \frac{R_i^2}{R_0^2} + \frac{R_i^2}{(R_i+d+x)^2} \right\} \quad (30)$$

In the sequel, we give a brief outline of the exterior collocation method, the details can be found in [6].

---

<sup>6</sup>HUSSAIN, M. A., HAGGERTY, R. G., PU, S. L., and NOBLE, B., "Exterior Collocation For Three Dimensional Surface Flaw", WVT-TR-75053, Watervliet Arsenal, Watervliet, N.Y., 1975.

The method of exterior collocation, for a symmetric surface flaw located on the plane  $z=0$ , requires construction of a set of functions which satisfy the mixed boundary conditions on the plane  $z=0$ . These conditions are: the normal stress is zero inside the crack-surface and normal displacement is zero outside the crack-surface. Symmetry of the problem further requires shearing stresses to vanish on the entire plane  $z=0$ . For the case of a circular flaw this was accomplished using three-dimensional Boussinesq potentials where the harmonic functions were represented by Kobayashi potentials (integral representation of potential functions) and superposition of such a solution with uniform field and plane strain solutions to satisfy the above boundary conditions. The results are:

$$\begin{aligned} \sigma_r &= \sum_n A_n (n(n+1)r^{-2}[(1-2\nu)I_1 - zI_2] - (I_3 - zI_4) - r^{-1}[(1-2\nu)I_5 - zI_6] \\ &\quad - \epsilon_n a^{-n-3/2} (n-2)(2n+1)\Gamma(n+1/2)r^n/[4\sqrt{2\nu}\Gamma(n+1)]) \cos n\theta, \\ \sigma_\theta &= \sum_n A_n (-n(n+1)r^{-2}[(1-2\nu)I_1 - zI_2] - 2\nu I_3 + r^{-1}[(1-2\nu)I_5 - zI_6] \\ &\quad + \epsilon_n a^{-n-3/2} (n+2)(2n+1)\Gamma(n+1/2)r^n/[4\sqrt{2\nu}\Gamma(n+1)]) \cos n\theta, \\ \sigma_z &= A_0 \sqrt{\pi/2} a^{-3/2} + \sum_n A_n (-I_3 - zI_4 + \epsilon_n a^{-n-3/2} (2n+1)\Gamma(n+1/2)r^n / \\ &\quad [\sqrt{2}\Gamma(n+1)]) \cos n\theta, \\ \tau_{r\theta} &= \sum_n \epsilon_n A_n (n(n+1)r^{-2}[(1-2\nu)I_1 - zI_2] - nr^{-1}[(1-2\nu)I_5 - zI_6] \\ &\quad + a^{-n-3/2} (2n+1)\Gamma(n+1/2)r^n/[4\sqrt{2\nu}\Gamma(n+1)]) \sin n\theta, \\ \tau_{rz} &= \sum_n A_n z[-nr^{-1}I_3 + I_7] \cos n\theta, \\ \tau_{\theta z} &= \sum_n -\epsilon_n A_n n z r^{-1} I_3 \sin n\theta. \end{aligned} \quad (31)$$

Where  $\epsilon_n=0$  for  $n=0$ ,  $\epsilon_n=1$  for  $n \neq 0$ , the summation  $\sum_n$  is over  $n=0, 1/2, 1, 3/2, \dots, \infty$  and  $A_n$ 's are constants to be determined by the collocation method. We have used the cylindrical coordinate system  $(r, \theta, z)$  with the origin located at the center of the circular crack of radius 'a', and  $I$ 's are integrals given below:

$$I_1 = \int_0^\infty k^{-2} J_n(kr) J_{n+3/2}(ka) k^{1/2} e^{-zk} dk, \\ I_2 = -\partial I_1 / \partial z, \quad I_3 = -\partial I_2 / \partial z, \quad I_4 = -\partial I_3 / \partial z \quad (32)$$

and

$$I_5 = \int_0^\infty k^{-1} J_{n-1}(kr) J_{n+3/2}(ka) k^{1/2} e^{-zk} dk \\ I_6 = -\partial I_5 / \partial z, \quad I_7 = -\partial I_6 / \partial z \quad (33)$$

After some basic integration, it can be shown from (31) above,

$$\sigma_z(z=0) = \begin{cases} 0, & r < a, \\ \frac{A_0}{a^{3/2}} \sqrt{\frac{\pi}{2}} + \sum_n A_n \left\{ \frac{\sqrt{2}}{\sqrt{\pi a}} \left(\frac{a}{r}\right)^n \left[ -\frac{1}{r} F\left(n+\frac{1}{2}, \frac{1}{2}; n+\frac{3}{2}; \frac{a^2}{r^2}\right) \right. \right. \\ \left. \left. + \frac{1}{\sqrt{r^2-a^2}} \right] + \epsilon_n \left(\frac{r}{a}\right)^n \frac{(2n+1)\Gamma(r+1/2)}{\sqrt{2a^3} \Gamma(n+1)} \right\} \cos n\theta, & r \geq a, \end{cases} \quad (34)$$

$$2Gu_z(z=0) = \begin{cases} 0, & \text{for } r > a, \\ 2\sqrt{2/\pi} (1-\nu)a^{-3/2}(a^2-r^2)^{1/2} \sum_n A_n (r/a)^n \cos n\theta, & r \leq a. \end{cases} \quad (35)$$

Hence it is seen from (33), (34) that the set of functions selected satisfy the mixed boundary conditions of the crack problem. The stress intensity factor can be computed from equation (34) or (35):

Table 3. Values of  $A_n$ 's for  $N=28$ ,  $\nu=0.3$  and  $a=1''$ ,  $d=0.3''$ ,  $TH=3.575''$ ,  $HW=3''$ ,  $HH=3''$  with Linear Constraint  $A_0 = -\sum A_n \cos n(\cos^{-1}(d/a))$

n	$A_n$	$A_{n+1/2}$
0	0.17074000 $\times 10^1$	- 0.28808100 $\times 10^2$
1	0.21008300 $\times 10^3$	- 0.72235200 $\times 10^3$
2	0.15196900 $\times 10^4$	- 0.21668300 $\times 10^4$
3	0.21888900 $\times 10^4$	- 0.15776100 $\times 10^4$
4	0.78043600 $\times 10^3$	- 0.22554700 $\times 10^3$
5	0.51905600 $\times 10^1$	0.24505900 $\times 10^2$
6	- 0.89767900 $\times 10^1$	0.17788400 $\times 10^1$
7	- 0.18092500 $\times 10^1$	0.16957900 $\times 10^1$
8	- 0.66020300 $\times 10^0$	- 0.28821800 $\times 10^{-1}$
9	0.13661300 $\times 10^0$	- 0.43773500 $\times 10^{-1}$
10	- 0.13656300 $\times 10^{-1}$	0.18752300 $\times 10^{-1}$
11	- 0.89871200 $\times 10^{-2}$	0.26154100 $\times 10^{-2}$
12	- 0.48300500 $\times 10^{-3}$	0.50154900 $\times 10^{-4}$
13	- 0.14393100 $\times 10^{-5}$	- 0.15544700 $\times 10^{-6}$

$$K_I = K_I(\theta) = \sqrt{2} a^{-1} \sum_n A_n \cos n\theta \quad (36)$$

once the  $A_n$ 's have been computed.

In general it is not possible to obtain  $A_n$ 's in the infinite series. An approximate solution, however, can be found by satisfying boundary conditions at  $m$  selected discrete points, called collocation points, on the remaining boundaries exterior to the plane of the crack. At each boundary point there are three boundary conditions. From the  $3m$  equations we can at most solve for  $3m$  unknown coefficients  $A_n$ 's. To avoid an illconditioned matrix, the boundary conditions are to be satisfied in a least square sense. Computationally, the least square procedure, in obtaining stable results, is to choose a rather large value of  $m$  and solve  $A_n$ 's from the  $N \times N$  system of 'normal equations', which are derived by minimizing the sum of the squares of errors at collocation points. Since the value of  $N$  is not known a priori, we solve the normal equations for  $N=1,2,\dots$  until the required stability is achieved in  $K_I$  and there is no significant change in 'residuals'. As explained in [6] there is an additional requirement for surface flaw problems; namely the boundary traction must vanish at points of the crack-free surface intersection. This gives a linear constraint on  $A_n$ 's (see Table 3) and leads to zero stress intensity factors at such points. With TH, HH, HW,  $a$ ,  $d$ ,  $v$ ,  $N$ , Figure 10, as input parameters and automatic generation of  $m$  nearly equally spaced collocation points, a computer program was

---

<sup>6</sup>HUSSAIN, M. A., HAGGERTY, R. G., PU, S. L., and NOBLE, B., "Exterior Collocation For Three Dimensional Surface Flaw", WVT-TR-75053, Watervliet Arsenal, Watervliet, N.Y., 1975.

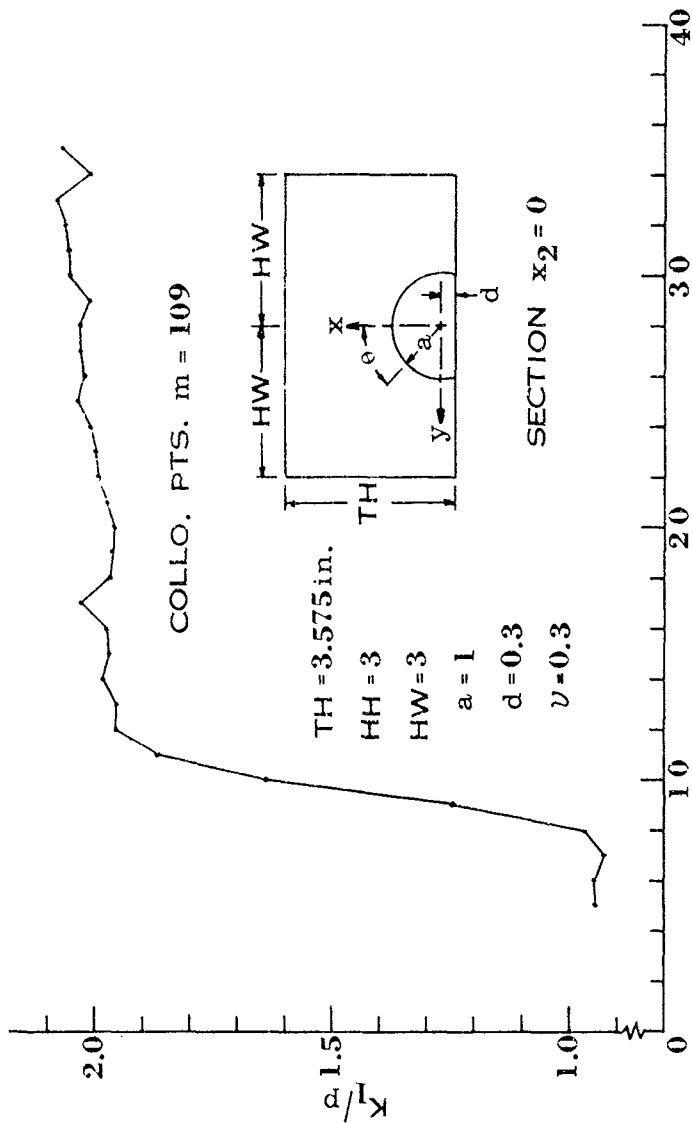


FIGURE 11. Graph of  $K_1/p$  vs  $N$  showing the stability of collocation results for  $N > 15$ .

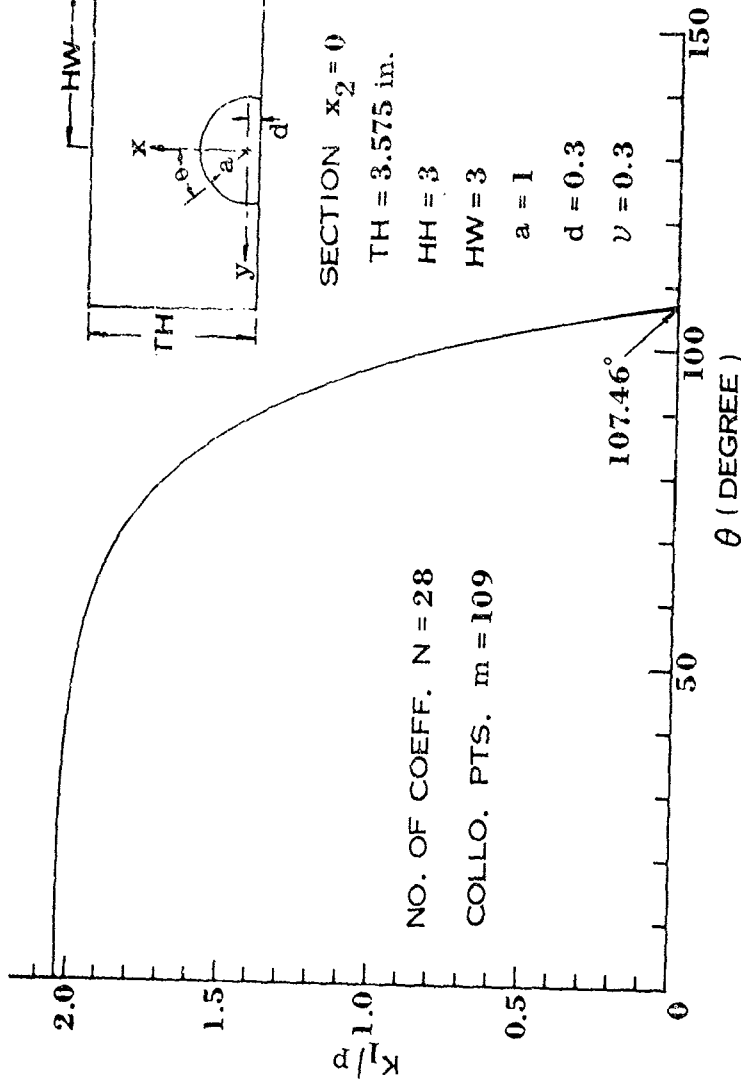


FIGURE 12. Graph of  $K_1/p$  vs  $\theta$  for  $N=28$  with 109 collocation points.

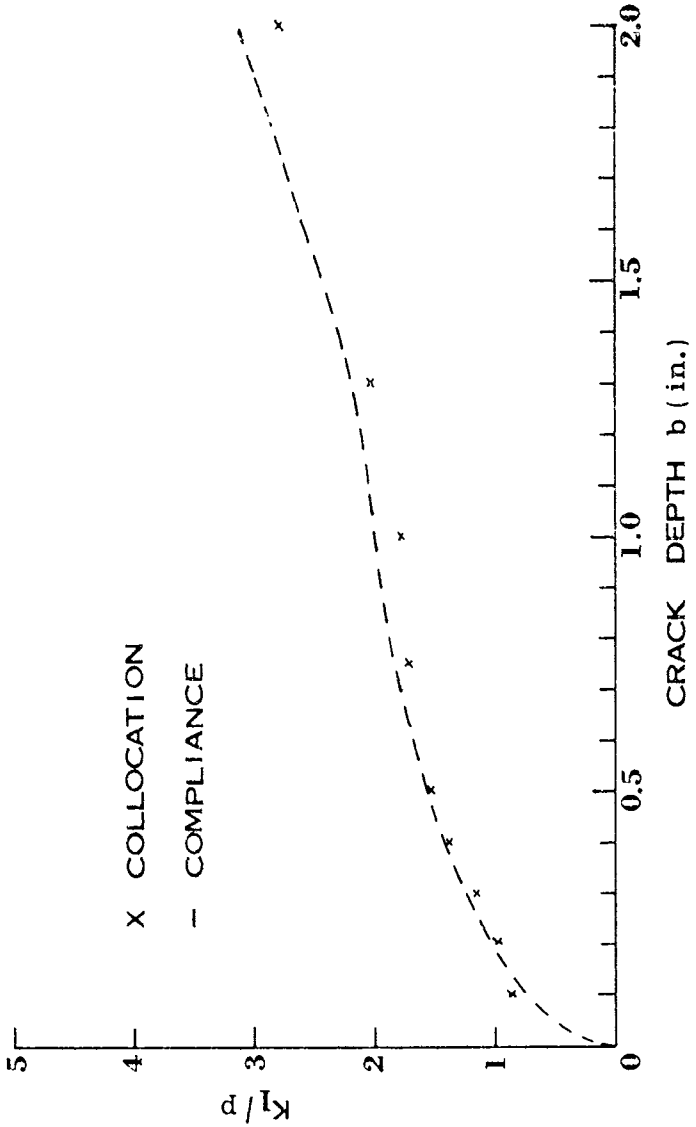


FIGURE 13. Graph of  $K_I/p$  vs  $b$ , obtained by compliance tests and collocation method for non-autofretage tube.

written which calculates  $A_n$ 's and the stress intensity factors as briefly described. (The symmetry of the problem allows us to work with half of the geometry.)

In Figure 11, we plot  $K_I/p$  vs  $N$ , up to  $N=35$ , showing the stability of the results. It is seen that the results are stable within 3-4% for  $N>15$ . In Figure 12, we plot  $K_I/p$  vs  $\theta$  for  $N=28$  with 109 collocation points. It is seen that  $K_I/p$  is maximum at  $\theta=0$  (i.e. at the deepest point of the crack) and vanishes at  $\theta=107.46^\circ$  (i.e. at points of the crack-free surface intersection). In Table 3, we list  $A_n$ 's for the above case showing convergences of  $A_n$  for large  $n$ . Similar computations were carried out for crack depths of  $b+a+d = .1, .2, .3, .4, .5, .75, 1.0, 1.3$  and  $2$ . inches. The results are shown in Figure 13. In the same figure, we have plotted  $K_I/p$  obtained by compliance results (see Figure 9). Excellent agreement is seen between the experimental and theoretical results.

#### CONCLUDING REMARKS

In this report we have developed a compliance calibration of a thick-walled circular cylinder with a symmetric internal surface flaw. Results obtained agree well, for small crack depths, to those obtained analytically for a semi-circular flaw by the collocation method.

#### REFERENCES

1. UNDERWOOD, J. H., LASSELLE, R. R., SCANLON, R. D. and HUSSAIN, M. A., "A Compliance K Calibration For A Pressurized Thick-Wall Cylinder With A Radial Crack" Engineering Fracture Mechanics, Vol. 4, 1972, pp. 231-244.
2. EMERY, A. F. and SMITH, F. W., "Some Basic Properties of Penny-Shaped Cracks" Mathematika, Vol. 13, 1966, pp. 172-180.
3. SOKOLNIKOFF, I. S., "Mathematical Theory of Elasticity" McGraw Hill Book Company, New York, 1956, p. 66.
4. AHLBERG, J. H., NILSON, E. N., WALSH, J. L., "The Theory of Splines and Their Applications," Academic Press, New York, 1967.
5. IRWIN, G. R., "Structural Aspect of Brittle Fracture," Applied Materials Research, Vol. 3, 65, 1964.
6. HUSSAIN, M. A., HAGGERTY, R. G., PU, S. L., and NOBLE, B., "Exterior Collocation For Three Dimensional Surface Flaw," WVT-TR-75053, Watervliet Arsenal, Watervliet, N. Y., 1975.

## APPENDIX A

A collocation analysis for simulated crack geometry was also carried out for the case of an autofrettaged tube. Due to the presence of compressive stress at the inner bore of the tube, it was reasonable to assume the loading condition as a superposition of applied and the residual stress fields. Hence, eq (30) was replaced by:

$$\sigma_z/p = 1 + \frac{1}{(1-a^2/b^2)} \left\{ \frac{a^2}{b^2} + \frac{a^2}{(a+d+x)^2} \right\} + \begin{cases} \frac{\sigma_y}{p\sqrt{3}} \left[ (2 \log \frac{a+d+x}{\rho} + 1 + \frac{\rho^2}{b^2}) - \left( \frac{a^2}{b^2} + \frac{a^2}{(a+d+x)^2} \right) (2 \log \frac{\rho}{a} + 1 - \frac{\rho^2}{b^2}) / (1 - \frac{a^2}{b^2}) \right], \\ \text{for } (a+d+x) \leq \rho \\ \frac{\sigma_y}{p\sqrt{3}} \left[ (\rho^2/b^2 + \rho^2/(a+d+x)^2) - (2 \log \rho/a + 1 - \rho^2/b^2) \right. \\ \left. (a^2/b^2 + a^2/(a+d+x)^2) / (1 - a^2/b^2) \right], \\ \text{for } (a+d+x) > \rho \end{cases} \quad (A-1)$$

where  $a=R_1$ ,  $b=R_0$ , are the inner and outer radii.  $\sigma_y$  the yield stress,  $p$  is the pressure and  $\rho$  is the interface depending upon the percentage of autofrettage (e.g., for 30% autofrettage  $\rho = a + 0.3(b-a)$ .) The results of such a computation for  $R_1=3.55"$   $R_0=7.125"$   $p=48,000$  psi,  $\sigma_y=170,000$  psi, and crack depths  $b = .125", .25", .5", .75", .9", 1", 1.25", 1.5", 1.75", 2"$  are plotted in Figure A1. It is seen that  $K_I/p$  is substantially lower for an autofrettaged tube as compared to a non-autofrettaged tube (Fig. 13). It is further seen that  $\frac{\partial K_I/p}{\partial b}$  is bounded as opposed to a non-autofrettaged tube at  $b=0$ .

The compliance test as previously explained was done for a 30% autofrettaged tube of the same dimensions as before. The change in the

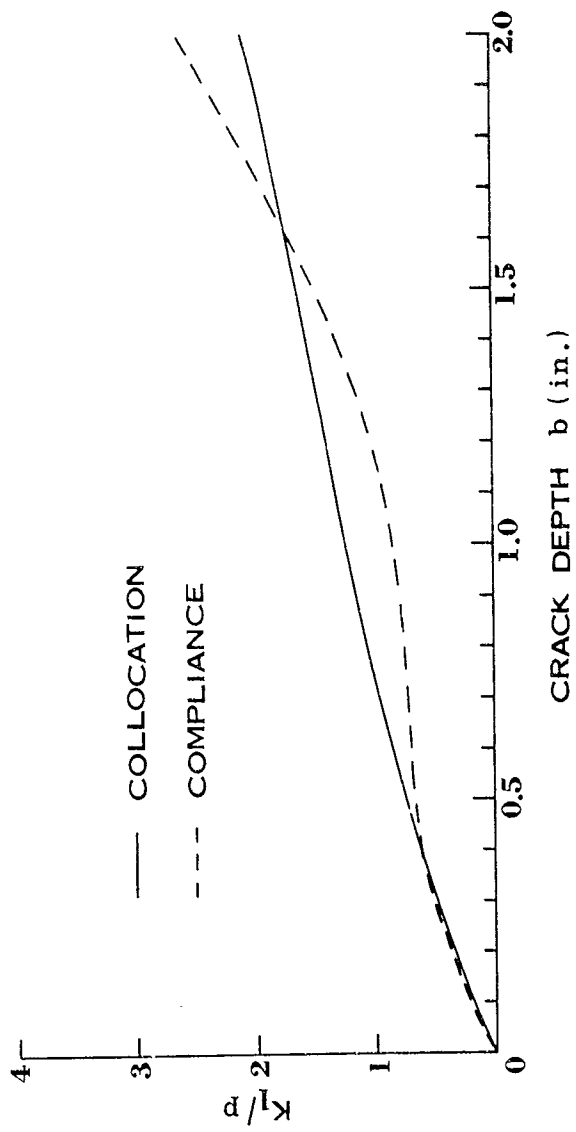


FIGURE A1. Graph of  $K_I/p$  vs  $b$  for 30% autofretted tube.

Table A1. Change in Cross-Section Area  $\Delta A_0$  (in<sup>2</sup>) for 30% Autofrettage Tube for Various Crack Depths at Sequential Pressure Levels

CRACK DEPTH b in.	PRESSURE p ksi									
	16	32	48	40	32	24	16	8	4	
.27	.1145803	.2301047	.3128709	.2853734	.2321038	.1719471	.1119808	.0517532	.0197426	
.275	.1179358	.2200602	.3355455	.2997712	.2391243	.1786646	.1180322	.0606015	.0288618	
.28	.1134774	.2330917	.3337949	.2912687	.2350314	.1751991	.1171726	.0569664	.0270394	
.35	.1191472	.2380425	.3578075	.2989941	.2393539	.1815514	.1229474	.0641659	.0320505	
.55	.1107011	.2286202	.3637151	.2945896	.2341506	.1749228	.1133022	.05579	.02459	
.81	.1103763	.2315766	.3484302	.2930064	.2309684	.1717835	.1130522	.039759	.0074058	
.98	.1131933	.2375365	.3590167	.3020805	.2422522	.1803832	.1219472	.0638284	.0317702	
1.5	.1183866	.2397103	.3546551	.3005621	.2416029	.1830562	.1219719	.0600471	.0314866	
2.0	.1220590	.2381759	.3756629	.3099292	.2453268	.1802772	.1152081	.0545379	.0235604	
2.5	.1203393	.2472155	.4010268	.3366706	.2706592	.2018517	.1317442	.0572565	.0233657	
3.0	.1434359	.2885957	.4374072	.3663048	.2985782	.2128523	.1382979	.0642105	.027231	

cross-sectional area was computed as before and the results for a few pressures are given in Table A1. It is immediately seen that the data is quite scattered for small crack depths. This may be due to the fact that the notch was put in before the autofrettage process or may be due to relaxation of residual stresses under cyclic loading in the presence of a notch. Neglecting the first three data points and extrapolating the data for zero crack depth to  $\Delta A_0 = .357 \text{ in}^2$  the stress intensity factors with  $h=1.0$  and  $\lambda=1000$  (less smoothing) were computed. The results are shown in Figure A1, together with the collocation data. Again, fairly good agreement is seen for small crack depths.

## WATERVLIET ARSENAL INTERNAL DISTRIBUTION LIST

May 1976

	<u>No. of Copies</u>
COMMANDER	1
DIRECTOR, BENET WEAPONS LABORATORY	1
DIRECTOR, DEVELOPMENT ENGINEERING DIRECTORATE	1
ATTN: RD-AT	1
RD-MR	1
RD-PE	1
RD-RM	1
RD-SE	1
RD-SP	1
DIRECTOR, ENGINEERING SUPPORT DIRECTORATE	1
DIRECTOR, RESEARCH DIRECTORATE	2
ATTN: RR-AM	1
RR-C	1
RR-ME	1
RR-PS	1
TECHNICAL LIBRARY	5
TECHNICAL PUBLICATIONS & EDITING BRANCH	2
DIRECTOR, OPERATIONS DIRECTORATE	1
DIRECTOR, PROCUREMENT DIRECTORATE	1
DIRECTOR, PRODUCT ASSURANCE DIRECTORATE	1
PATENT ADVISORS	1

## EXTERNAL DISTRIBUTION LIST

May 1976

1 copy to each

CDR  
 US ARMY MAT & DEV READ. COMD  
 ATTN: DRCRD  
       DRCRD-TC  
       DRCRD-W  
 5001 EISENHOWER AVE  
 ALEXANDRIA, VA 22304

OFC OF THE DIR. OF DEFENSE R&E  
 ATTN: ASST DIRECTOR MATERIALS  
 THE PENTAGON  
 WASHINGTON, D.C. 20315

CDR  
 US ARMY TANK-AUTMV COMD  
 ATTN: AMDTA-UL  
       AMSTA-RKM MAT LAB  
 WARREN, MICHIGAN 48090

CDR  
 PICATINNY ARSENAL  
 ATTN: SARPA-TS-S  
       SARPA-VP3 (PLASTICS  
       TECH EVAL CEN)  
 DOVER, NJ 07801

CDR  
 FRANKFORD ARSENAL  
 ATTN: SARFA  
 PHILADELPHIA, PA 19137

DIRECTOR  
 US ARMY BALLISTIC RSCH LABS  
 ATTN: AMXBR-LB  
 ABERDEEN PROVING GROUND  
 MARYLAND 21005

CDR  
 US ARMY RSCH OFC (DURHAM)  
 BOX CM, DUKE STATION  
 ATTN: RDRD-IPL  
 DURHAM, NC 27706

CDR  
 WEST POINT MIL ACADEMY  
 ATTN: CHMN, MECH ENGR DEPT  
 WEST POINT, NY 10996

CDR  
 US ARMY ARMT COMD  
 ATTN: AMSAR-PPW-IR  
       AMSAR-RD  
       AMSAR-RDG  
 ROCK ISLAND, IL 61201

CDR  
 US ARMY ARMT COMD  
 FLD SVC DIV  
 ARMCOM ARMT SYS OFC  
 ATTN: AMSAR-ASF  
 ROCK ISLAND, IL 61201

CDR  
 US ARMY ELCT COMD  
 FT MONMOUTH, NJ 07703

CDR  
 REDSTONE ARSENAL  
 ATTN: AMSMI-RRS  
       AMSMI-RSM  
 ALABAMA 35809

CDR  
 ROCK ISLAND ARSENAL  
 ATTN: SARRI-RDD  
 ROCK ISLAND, IL 61202

CDR  
 US ARMY FGN SCIENCE & TECH CEN  
 ATTN: AMXST-SD  
 220 7TH STREET N.E.  
 CHARLOTTESVILLE, VA 22901

DIRECTOR  
 US ARMY PDN EQ. AGENCY  
 ATTN: AMXPE-MT  
 ROCK ISLAND, IL 61201

CDR  
 HQ, US ARMY AVN SCH  
 ATTN: OFC OF THE LIBRARIAN  
 FT RUCKER, ALABAMA 36362

EXTERNAL DISTRIBUTION LIST (Cont)

1 copy to each

CDR  
US NAVAL WPNS LAB  
CHIEF, MAT SCIENCE DIV  
ATTN: MR. D. MALYEVAC  
DAHLGREN, VA 22448

DIRECTOR  
NAVAL RSCH LAB  
ATTN: DIR. MECH DIV  
WASHINGTON, D.C. 20375

DIRECTOR  
NAVAL RSCH LAB  
CODE 26-27 (DOCU LIB.)  
WASHINGTON, D.C. 20375

NASA SCIENTIFIC & TECH INFO FAC  
PO BOX 8757, ATTN: ACQ BR  
BALTIMORE/WASHINGTON INTL AIRPORT  
MARYLAND 21240

DEFENSE METALS INFO CEN  
BATTELLE INSTITUTE  
505 KING AVE  
COLUMBUS, OHIO 43201

MANUEL E. PRADO / G. STISSER  
LAWRENCE LIVERMORE LAB  
PO BOX 808  
LIVERMORE, CA 94550

DR. ROBERT QUATTRONE  
CHIEF, MAT BR  
US ARMY R&S GROUP, EUR  
BOX 65, FPO N.Y. 09510

2 copies to each

CDR  
US ARMY MOB EQUIP RSCH & DEV COMD  
ATTN: TECH DOCU CEN  
FT BELVOIR, VA 22060

CDR  
US ARMY MAT RSCH AGCY  
ATTN: AMXMR - TECH INFO CEN  
WATERTOWN, MASS 02172

CDR  
WRIGHT-PATTERSON AFB  
ATTN: AFML/MXA  
OHIO 45433

CDR  
REDSTONE ARSENAL  
ATTN: DOCU & TECH INFO BR  
ALABAMA 35809

12 copies

CDR  
DEFENSE DOCU CEN  
ATTN: DDC-TCA  
CAMERON STATION  
ALEXANDRIA, VA 22314

NOTE: PLEASE NOTIFY CDR, WATERVLIET ARSENAL, ATTN: SARVV-RT-TP,  
WATERVLIET, N.Y. 12189, IF ANY CHANGE IS REQUIRED TO THE ABOVE.